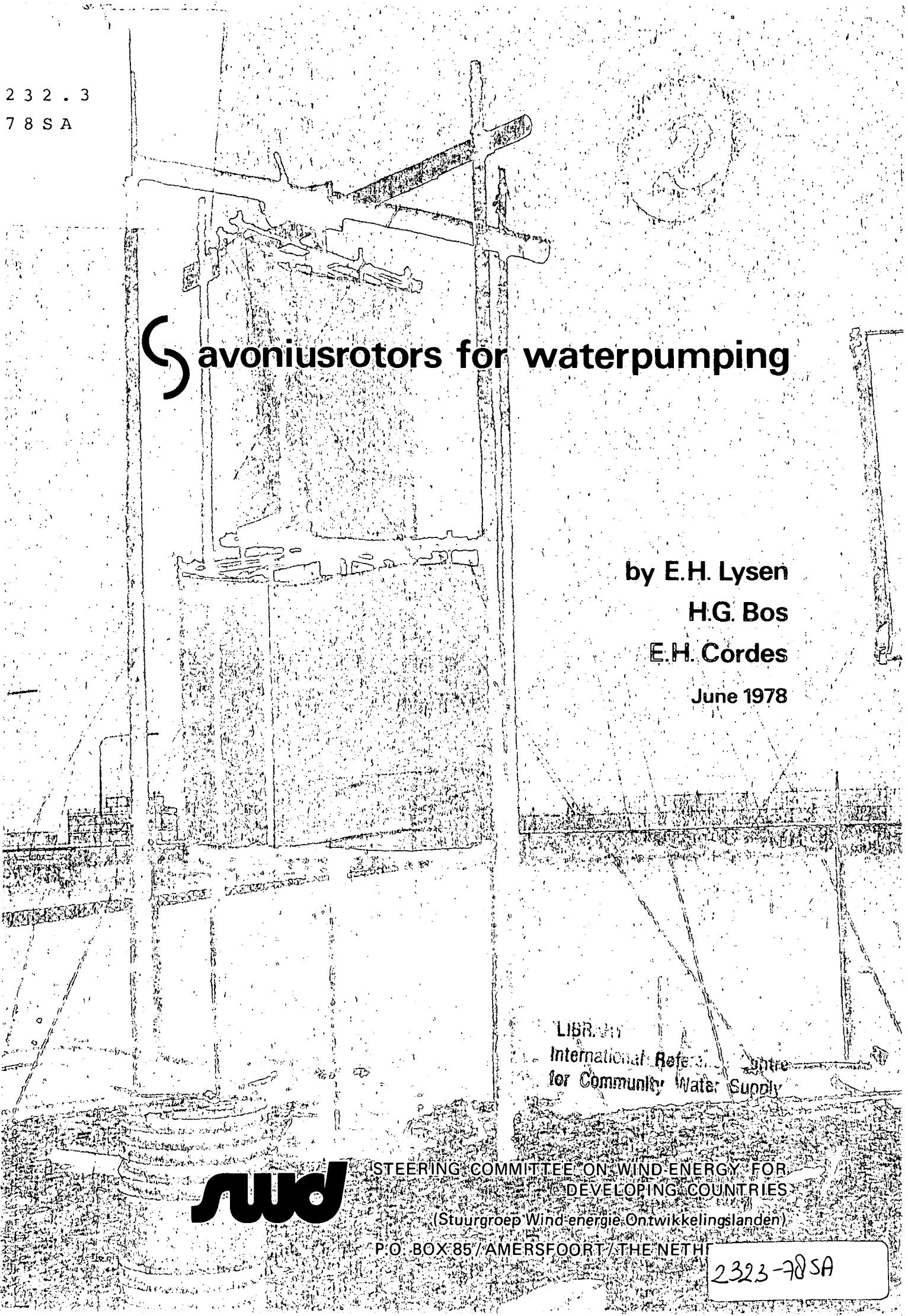

Savoniusrotors for waterpumping

by E.H. Lysen
H.G. Bos
E.H. Cordes

June 1978

STEERING COMMITTEE ON WIND ENERGY FOR DEVELOPING COUNTRIES
(Stuurgroep Wind-energie Ontwikkelingslanden)
P.O. BOX 85 / AMERSFOORT / THE NETH

SAVONIUSROTORS FOR WATERPUMPING

by E.H. Lysen
H.G. Bos
E.H. Cordes

State University Groningen
Technical Physics Laboratories

june 1978

Steering Committee Wind Energy for Developing Countries
P.O. Box 85 / Amersfoort / The Netherlands

PUBLICATION SWD 78 – 2

This publication was realized under the auspices of the Steering Committee on Wind-energy for Developing Countries S.W.D., by a team of the Technical Physics Laboratories of the State University Groningen.
The S.W.D. is financed by the Netherlands Ministry for Development Cooperation and is staffed by:

the State University Groningen (till 30-6-1978),
the Eindhoven University of Technology,
the Twente University of Technology,
the Netherlands Organization for Applied Scientific Research, and
DHV, Consulting Engineers, Amersfoort

and collaborates with other interested parties.

The S.W.D. tries to help governments, institutes and private parties in the Third World, with their efforts to use wind-energy and in general to promote the interest for wind-energy in Third World Countries.

CONTENTS

ABSTRACT

This report explores some facets of the use of Savoniusrotors for water-pumping, particularly for application in developing countries:

1. The design parameters of the optimum Savoniusrotor as deduced from literature data.
2. A theoretical analysis of the coupling of a low speed windrotor with a constant torque piston pump. The inefficient use of the available rotorpower at higher windspeeds is clearly demonstrated.
3. Open air measurements on a full scale Savoniusrotor with blades in the form of a sail curved around a number of supporting rods. Sails are chosen because they offer the possibility of reefing the sails before storms and because they are relatively cheap.
4. The construction of a double Savoniusrotor, made out of wood, sails and ropes only, driving a commercial membrane pump.

We conclude that Savoniusrotors with sails offer a relatively simple and safe solution to pump moderate amounts of water in developing countries, but that the design we choose to test has rather poor characteristics in comparison with similar foreign designs.

NOMENCLATURE

A	swept area of rotor (2RH)	m^2
a	chord length of rotorblade	m
b	diameter of rotoraxis	m
c	camberdepth of rotorblade	m
C_P	powercoefficient	-
C_Q	torquecoefficient	-
d	diameter of rotor	m
H	height of rotor	m
h	height of rotorblade	m
L	length of rotoraxis	m
N	number of analog signals to microprocessor	-
P	power	W
Q	torque	Nm
R	radius of rotor	m
Re	Reynoldsnumber (related to d)	-
r	radius of curvature of rotorblades	m
s	gapwidth of rotor	m
t	minimum sampling period of microprocessor	s
V_o	design windspeed for $C_P = C_{Pmax}$	m/s
V_∞	undisturbed windspeed	m/s

λ	tipspeedratio	-
λ_o	tipspeedratio at $C_P = C_{Pmax}$	-
ρ	density of air	kg/m^3
Ω	rotational speed	1/s

1. INTRODUCTION

In 1924 Sigurd J. Savonius constructed his first wing rotor, mainly to propel sailing vessels. The successful crossing of the Atlantic by Flettner's rotor ship the "Buckau" (driven by the Magnus force on two large rotating cylinders) led Savonius to the idea to split the cylinders in two halves so the wind would drive the cylinders and no external power would be needed at all.

Windtunnel tests showed that a small overlap between the inner blade edges, having an air gap, gave a much improved performance. Afterwards many windtunnel tests have been carried out on small Savonius rotors, however, without a common agreement on optimum shape (see chapter 2).

Open air measurements are rarely to be found in the literature. Savonius himself observed a 5% increase in power output in natural wind in comparison to his windtunnel results [1], but no confirmation is to be found. Most often one refers to the oil drum rotor of Brace Research Institute[9], which gave a modest power coefficient of 0.14 Frenkel[2]. (ITDG) reports the poor performance of waterpumping Savoniusrotors at Omo Station (Ethiopia) in comparison to Cretan-type sail wind mills. Barnhart[11] describes a triple Savonius rotor, following Hackleman, both without mentioning results. Govinda Raju, however, seems successful with his sailtype Savonius rotor driving a tyre-pump[14]. Encouraging results are also obtained by the International Rice Research Institute in the Philippines. They tested (1977) a dozen Savoniusrotors, made out of oil drum sheet, at different places in the Philippines, to be used for irrigation purposes.

To be able to assess the potential of Savonius rotors to drive water pumps, especially for developing countries, we tested several Savonius rotors with sails in natural winds. The main reason to use sails is the possibility to "reef" the sails, when storm is coming up. Further we constructed one full scale rotor with only wood, ropes and sails. The metal rotors are well described in the literature[12, 18] and in several parts of the developing countries wood and ropes are easier available than bolts, metal bearings and pipes.

2. THE OPTIMUM SAVONIUS ROTOR

A comparison of the published windtunnel measurements reveals no general consensus about the design parameters of an aerodynamically optimum Savonius rotor. In this respect we call the rotor with the highest power coefficient the optimum Savonius rotor. In practice accounting other parameters, such as materials consumption, structural simplicity, and minimum costs will result in other optimum shapes.

Part of the differences in windtunnel measurements stem from a different interpretation of the results. Especially when the swept area of the rotor is more than, let's say, 5% of the tunnel cross sectional area and blockage corrections have to be made, large deviations occur[15].

Only one thing seems to be rather clear: the number of blades must be two. Tests by Sivasegaram[3] and Shankar[4] indicate that a two bladed rotor has a 30% to 50% higher peak power coefficient than a three bladed rotor. Sandia Laboratories arrived at the same results: C_p=0.14 to 0.17 for the three-bladed versus C_p=0.25 for the two-bladed rotor[13, 17].

For discussion of the other relevant parameters we will refer to Fig. 1.

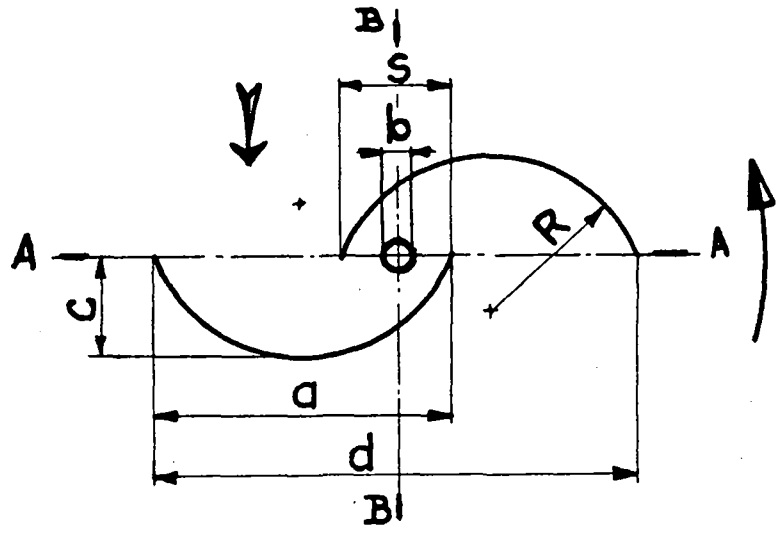

FIG. 1. Relevant parameters to describe a Savonius rotor with cylindrical shaped blades.

The optimum gap width-diameter ratio $\frac{S}{d}$ varies between $\frac{1}{11}$ (Newman[5]), $\frac{1}{15}$ (Collin and Simpson[6]) and "no difference" between $\frac{1}{10}$ and $\frac{1}{20}$ (Shankar[4]).

Blake[7] remarks that a smaller gap gives lower efficiency but at the other hand a larger swept area. Indeed, Shankar's measurements indicate that the loss in efficiency is just about compensated by the increase in swept area, so the power remains the same. Starting torque, however, drops considerably. The "no gap" rotor has 40% (Shankar) or 15% (Sandia, 17) less starting torque.

The overlap of the blades near the gap is mostly zero, i.e. the blades do not cross the line A-A (see Fig. 1). Only Sivasegaram[3] gives his asymmetrical blades a larger overlap, but he does not mention any special influence of this overlap. Bach tested one group of rotors with a wider gap: the inner edges ended already at the line B-B perpendicular to A-A. They gave a 50% lower power coefficient.

The aspect ratio $\frac{h}{d}$ (height/diameter) is seldom optimized. Shankar[4] uses an aspect ratio of 0.35, Bach[8] uses 2, Carver and Mc Pherson[1] used 5.75 but concluded that $\frac{h}{d} = 2$ gave a "substantially" higher overall efficiency. The oildrum rotor of Simonds and Bodek[9] has an aspect ratio of 1.9. Wilson c.s.[15] predict a strong influence of aspect ratio, the higher the better, even above $\frac{h}{d} = 10$.

A central supporting column in the airgap is mostly omitted, because small models do not need it for structural strength. Shankar[4] reports a "negligible" effect of a column diameter/gap width ratio $\frac{b}{s} = 0.2$. No higher ratios are tested.

The effect of using extra guiding vanes is reported by Kentfield[10]. See also Fig. 2.

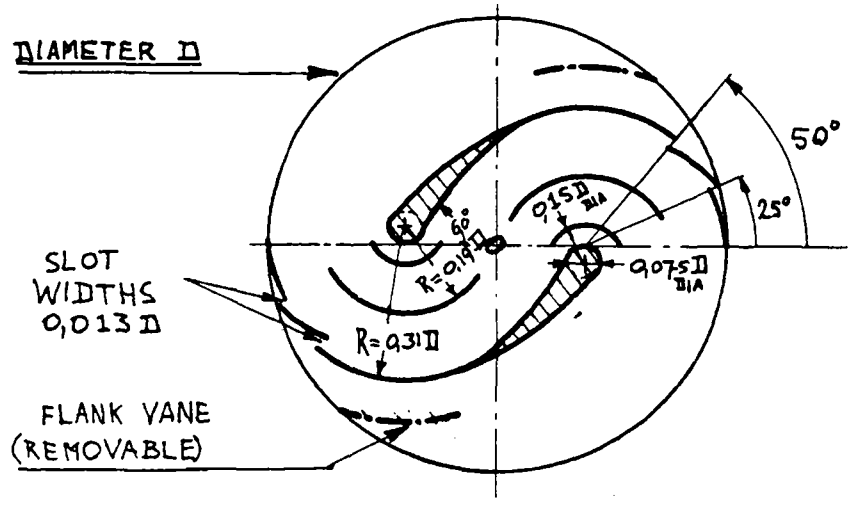

FIG. 2. A modified Savonius rotor, tested by Kentfield[10].

His modified rotor, without flank vanes gave a substantially higher starting torque. He reports an increase with a factor of three, but this is the result of extrapolation below $\lambda = 0.3$. A factor of two seems reasonable. This high starting torque has to be paid with a 25% lower power coefficient, which peaks at $\lambda = 0.6$.

The use of leading edge slots and trailing edge flaps (Fig. 2) improves the flow at low tip speed ratios. At tip speed ratios around unity they seem to become an extra drag source.

The curvature of the blades is mostly semi-circular, i.e. a = 2r (Fig. 1)*). Bach[8] already found an increased rotor performance with blades of assymmetrical section (C_p=0.24 versus C_p=0.225 with semicircular blades). This is confirmed by work at IRRI (Philippines) and by the investigations of Sivasegaram. The latter suggests a part of a spiral as the optimum blade curvature.

Shankar tested a rotor with shallower, but symmetrical blades with a = 1.6 x r. They gave a 25% drop in power coefficient, but a 10% higher starting torque, compared to the best rotor with semi-circular blades.

The curvature of the blades is important, not only for a maximum efficiency but also for a minimum material consumption. For circular blades the blade length is determined by the following formula:

$$\text{blade length} = 2\,r \arcsin \frac{a}{2r} \quad (\arcsin \text{ in radians}).$$

Shankar's rotor with a = 1.6r gives a 41% lower blade length than the rotor with a = 2r.

Wilson c.s.[15] predict a strong influence of curvature: for an aspect ratio of 1.25 and Re = 1.9×10^5 an a = 1.6r rotor (camber 0.25) gives C_{Pmax}=0.14, while an a =1.88r rotor (camber 0.35) gives C_p=0.21.

End plates are necessary to prevent air leakage at the upper and lower edges of the blades, thus sustaining a pressure build-up inside the blades. Removal of end plates results in a more than 50% lower power coefficient (Govinda Raju[14]). No research is carried out, as far as we know of, to see which percentage of the plate can be removed with how much power loss. Mostly one uses end plates with diameters 20% to 30% larger than d.

*) Sometimes the camber of a blade is defined as $\frac{c}{a} = \frac{r - \sqrt{r^2 - \frac{1}{4}a^2}}{a}$. For a = 2r the camber is $\frac{1}{2}$, while for a = 1.6 r the camber becomes 0.25.

The influence of Reynolds number (or higher wind speeds) is a strong one: higher Reynolds numbers give a better performance. This is why we seldom mentioned power coefficients, they all depend on the wind speed used. Shankar reports a C_P=0.19 for Re=10^5 and C_P=0.23 for Re=2x10^5. He uses a kinematic viscosity of v = 15,5 x 10^{-6} so the Reynolds formula becomes:

$$Re = 64.500.V_\infty.d.$$

Newman reports for his $\frac{S}{d} = \frac{1}{11}$ semicircular rotor an (uncorrected) C_P=0.24 for Re=10^5 and C_P=0.30 (uncorrected) for Re = 1.5 x 10^5. He mentiones that the increased performance can be attributed partly to outward flow along the concave sides of the blades for practically all orientations of the rotor.

The theoretical predictions of Wilson c.s.[15] result in a less pronounced influence of Reynolds number. This is probably true for the higher Reynolds numbers: Sandia reports the same C_{Pmax}=0.26 for Re = 4.3 x 10^5 and Re = 8.7 x 10^5 ($\frac{S}{d}$ = 0.1 and $\frac{h}{d}$ = 1.5).

CONCLUSION: The optimum Savonius rotor seems to have the following characteristics:

number of blades	2	aspect ratio	2 or higher
gap width-diameter ratio	$\frac{1}{10} - \frac{1}{20}$	curvature of blades	asymmetrical
blade overlap	zero	end plates	yes

This should result in a maximum power coefficient of about 0.20 at λ = 0.8 and Re = 1.5 x 10^5. The average starting torque will be C_Q=0.3 with a peak of 0.7 if the wind enters a blade under an angle of about 30° with respect to the line A-A (Fig. 1).

REMARK: The rather strong torque fluctuations during one revolution are cancelled out by placing two (or even three) Savoniusrotors on top of each other. Their axes of symmetry then must be turned over 90° (or 60° for three rotors).

3. THEORY OF COUPLING A WINDROTOR TO A RECIPROCATING PUMP

Most waterpumping windmills are coupled to a reciprocating piston pump. These pumps, however, demand a relatively constant torque whereas the rotor delivers a quadratic torque as a function of the wind velocity. The immediate result is that most windmill-pump combinations work at very low overall efficiencies.

Savoniusrotors, American multiblade windrotors and Chinese windrotors all possess a nearly parabolic C_P-λ curve, thus a linear C_Q-λ curve (Fig. 3).

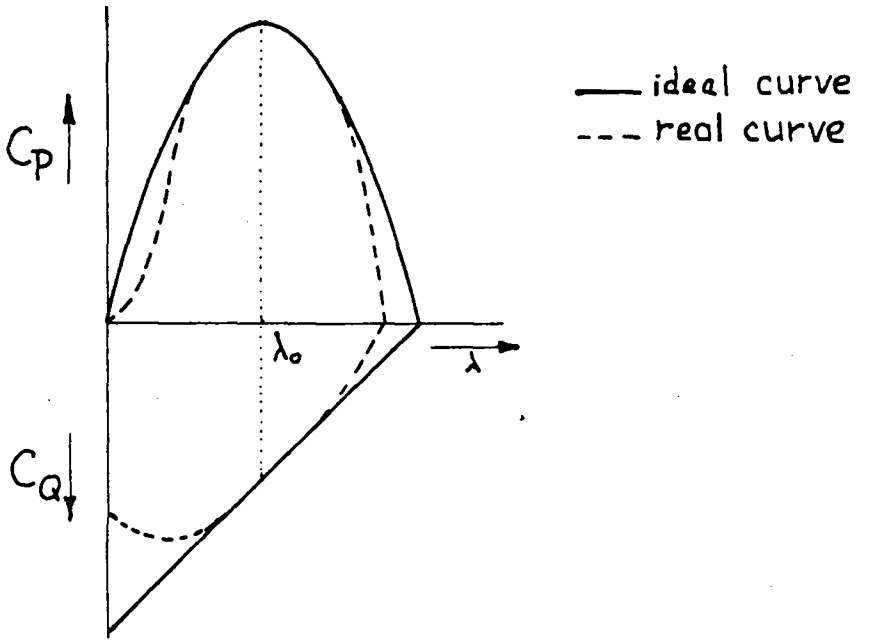

FIG. 3. Power and torque curve (dimensionless) of a slow running windrotor.

In this chapter first the idealized combination of a pump with constant torque coupled to a rotor with a linear C_Q-λ curve will be treated analytically. In reality the torque of a reciprocating pump varies during a revolution. Besides, in reality the characteristics deviate more or less from quadratic resp. linear curves (Fig. 3). In the second part of this chapter we will deal with the influence of these factors on the starting properties of the pump-windmill combination.

I. Idealized situation

Assume a pump which operates at 100% efficiency and constant torque:

$$\text{Torque:} \quad Q_{pump} = \text{constant} \tag{1}$$

$$\text{Power :} \quad P_{pump} = Q_{pump} \cdot \Omega \tag{2}$$

For a rotor with quadratic C_P-λ curve we use the following algebraic expressions:

$$\text{Torque:} \quad Q_{rotor} = C_Q \cdot \tfrac{1}{2} \rho A R V^2 \tag{3}$$

$$\text{Power :} \quad P_{rotor} = C_P \cdot \tfrac{1}{2} \rho A V^3 \tag{4}$$

$\lambda = \lambda_o$ for $C_P = C_{Pmax}$.

$$\text{Torque coefficient:} \quad C_Q = - \frac{C_{Pmax}}{\lambda_o} \left[\frac{\lambda}{\lambda_o} - 2 \right] \tag{5}$$

$$\text{Power coefficient :} \quad C_P = - C_{Pmax} \left[\left(\frac{\lambda}{\lambda_o} \right)^2 - 2 \frac{\lambda}{\lambda_o} \right] \tag{6}$$

Crucial now is the assumption that the windrotor-pump combination is designed to deliver C_{Pmax} at a certain windspeed $V=V_o$, operating than at $\lambda = \lambda_o$. At this windspeed V_o the following torque will be delivered by the rotor

$$Q(V_o) = \frac{C_{Pmax}}{\lambda_o} \cdot \tfrac{1}{2} \rho A R V_o^2 \tag{7}$$

This torque remains constant also for other wind speeds because this is exactly the torque the pump demands.
From (3) and (5) we find the general expression for the torque delivered by the rotor:

$$Q(V) = - \frac{C_{Pmax}}{\lambda_o} \left[\frac{\lambda}{\lambda_o} - 2 \right] \cdot \tfrac{1}{2} \rho A R V^2 \tag{8}$$

We now can derive the following expressions:

A. Equating (7) and (8) results in

$$\frac{\lambda}{\lambda_o} = 2 - \left(\frac{V}{V_o} \right)^{-2} \tag{9}$$

B. With the aid of (9) and the relations $\lambda = \frac{\Omega R}{v}$ and $\lambda_o = \frac{\Omega_o R}{V_o}$ we find:

$$\frac{\Omega}{\Omega_o} = 2\left(\frac{V}{V_o}\right) - \left(\frac{V}{V_o}\right)^{-1} \qquad (10)$$

C. The power output in general is given by $P = Q\Omega$. Q being constant we find with the aid of (10):

$$\frac{P}{P_o} = \frac{Q\Omega}{Q\Omega_o} = \frac{\Omega}{\Omega_o} = 2\left(\frac{V}{V_o}\right) - \left(\frac{V}{V_o}\right)^{-1} \qquad (11)$$

$\frac{P}{P_o}$ is drawn as a function of $\frac{V}{V_o}$ in Fig. 4.

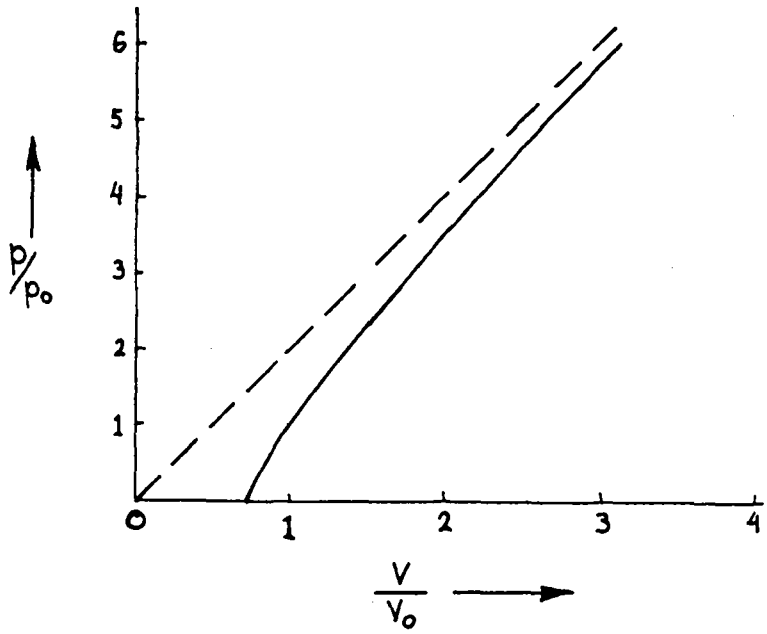

FIG. 4. Pumping power of a windrotor-pump combination as a function of windvelocity (pumping power and wind velocity both in multiples of the corresponding design parameters P_o resp. V_o).

D. From (6) and (9) we derive:

$$\frac{C_P}{C_{Pmax}} = \left(\left(\frac{\lambda}{\lambda_o}\right)^2 - 2\frac{\lambda}{\lambda_o}\right) = 2\left(\frac{V}{V_o}\right)^{-2} - \left(\frac{V}{V_o}\right)^{-4} \qquad (12)$$

This relation is shown in Fig. 5.

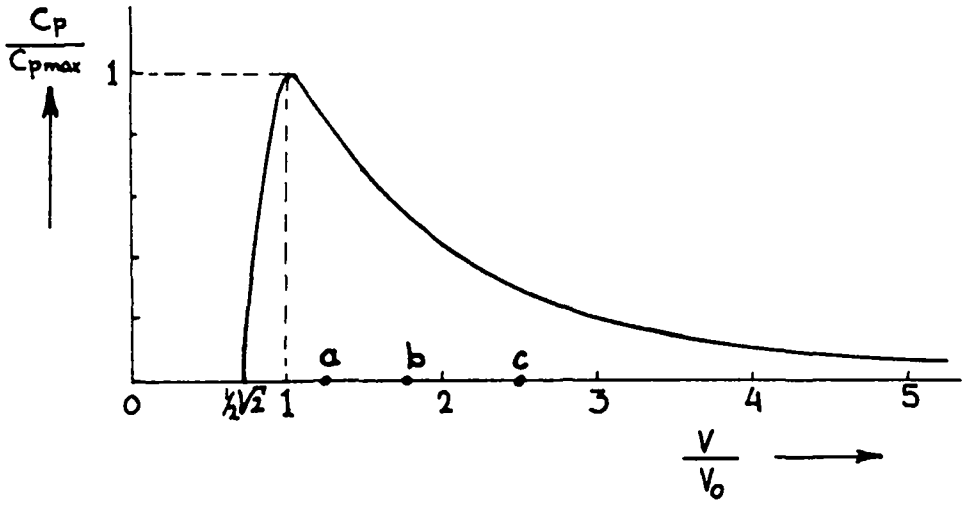

FIG. 5. The total power coefficient of a windrotor coupled to a reciprocating pump. The starting point a, baud c are given for a single acting pump coupled to rotors with λ_o=1,2 and 4 respectively and C_{Pmax} = 0.3.

It is evident from this figure that the windmill-pump combination mostly works at rather low efficiencies, the lower the higher the wind speed.

E. From relation (11) we see that the combination will deliver water if

$$V > \tfrac{1}{2}\sqrt{2}\, V_o \qquad (13)$$

II. Real situation

In real situations Q_{pump} is not constant during a revolution, nor are the C_P-λ and C_Q-λ curves of the rotor parabolic resp. linear. Both circumstances have a considerable influence on the starting properties of the windrotor-pump combination (Fig. 3).

A. Influence of a real pump characteristic on the starting properties. The torque of a single acting reciprocating pump is drawn in Fig. 6. The maximum torque is given by:

single acting	$Q_{max} = \pi \cdot Q_{pump}$	
double acting	$Q_{max} = \frac{\pi}{2} \cdot Q_{pump}$	
general	$Q_{max} = \alpha \cdot Q_{pump}$	$(\alpha > 1)$ (14)

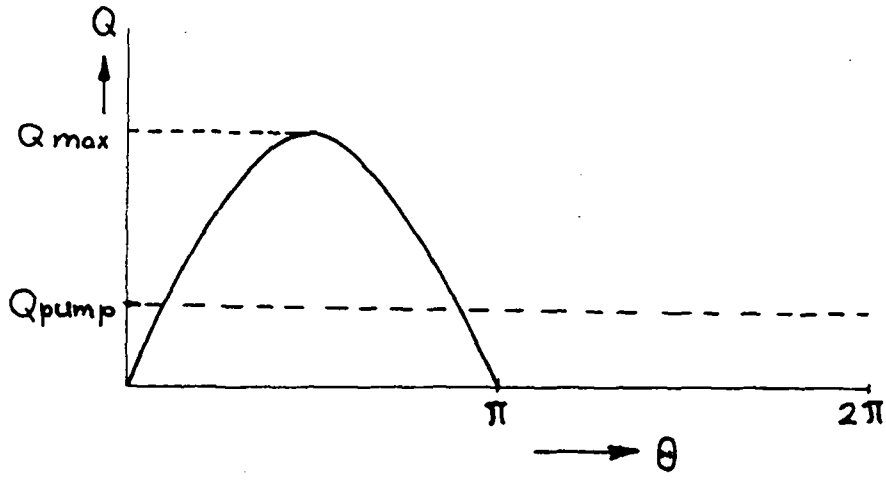

FIG. 6. Torque of a single acting reciprocating pump. One complete cycle is indicated by an angle of 2π radians (360°).

The starting condition is:

$$Q_{rotor} = \alpha\, Q_{pump} = Q_{start} .$$

Combining (7) and (8) gives with (14):

$$2\,\frac{C_{Pmax}}{\lambda_o} \cdot \tfrac{1}{2}\,\Omega\,AR\,V_{start}^2 = \alpha\,\frac{C_{Pmax}}{\lambda_o} \cdot \tfrac{1}{2}\,\Omega\,AR\,V_o^2$$

$$\text{or}\quad \frac{V_{start}}{V_o} = \sqrt{\frac{\alpha}{2}} \qquad (15)$$

Thus for a single acting pump $\frac{V_{start}}{V_o} = 1.25$ and for a double acting pump $\frac{V_{start}}{V_o} = 0.89$.

B. Influence of real C_P-λ and C_Q-λ curves on the starting properties.

In reality a C_Q-λ curve is not a straight line, but drops if $\lambda \to 0$ (Fig. 3). A rough approximation of $C_{Q,o}$ for horizontal axis rotors is given by:

$$C_{Q,o} = \frac{0.6}{\lambda_o^2} \qquad (16)$$

By substituting (16) in (3) and combining with (7) and (14) we find ($\lambda = 0$):

$$\frac{0.6}{\lambda_o^2} \cdot \tfrac{1}{2} \Omega AR\, V_{start}^2 = \alpha \frac{C_{Pmax}}{\lambda_o} \cdot \tfrac{1}{2} \Omega AR\, V_o^2$$

$$\text{or } \frac{V_{start}}{V_o} = \sqrt{\frac{\alpha \cdot \lambda_o \cdot C_{Pmax}}{0.6}} \qquad (17)$$

$C_{Pmax} = 0.3$ at $\lambda_o = 1$ and will rise for increasing λ_o-values to about 0.45.

Using $C_{Pmax} = 0.3$ gives:

$$\frac{V_{start}}{V_o} = \sqrt{\frac{\alpha\lambda_o}{2}} \simeq 0.71 \sqrt{\alpha\lambda_o}$$

With $C_{Pmax} = 0.45$ we find:

$$\frac{V_{start}}{V_o} = \sqrt{\frac{3}{4}\alpha\lambda_o} \simeq 0.87 \sqrt{\alpha\lambda_o}$$

We compute the following table for $\frac{V_{start}}{V_o}$ in a real situation:

	single acting pump		double acting pump	
λ_o	$C_{Pmax} = 0.3$	$C_{Pmax} = 0.45$	$C_{Pmax} = 0.3$	$C_{Pmax} = 0.45$
1	1.25	1.53	0.89	1.09
2	1.77	2.17	1.25	1.53
4	2.51	3.07	1.77	2.17
8	3.54	4.34	2.51	3.07

The starting points of a single acting pump $C_{Pmax} = 0.3$ are shown in fig. 5.

4. TEST RESULTS OF OPEN AIR MEASUREMENTS

The teststand is described in appendix I. The shape of the sails is chosen to be an approximation of Bach's[8] non-circular rotor form (Fig. 7). This form is chosen because of an approximation of this form is possible with less masts than the circular form. The non-circular form has the additional advantage of a smaller sail area. We tried to reach an acceptable approximation by means of 5 masts (Fig. 8). The masts are numbered from 1 up to 5 inclusive. Test results were obtained for two variables, first the influence of the number of masts, and secondly the effect of end plates.

FIG. 7. The shape of Bach's non-cylindrical blade.

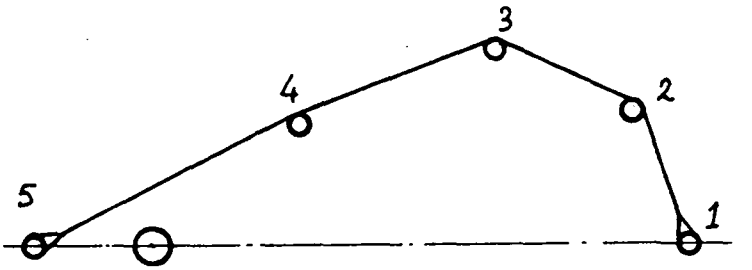

FIG. 8. Shape of a blade of our approximation of Bach's non-cylindrical blade.

The influence of the masts

We have tested a number of configurations. They are shown schematically in Fig. 9 (a to d).

a) Rotor with masts 1, 3 and 5.

The rotor initially oscillates. At a certain moment the rotor will start rotating due to variations in wind speed and direction. The angular speed remains low and little loading causes a stop of the mill. The oscillation is caused by the sail area between masts 1 and 3.

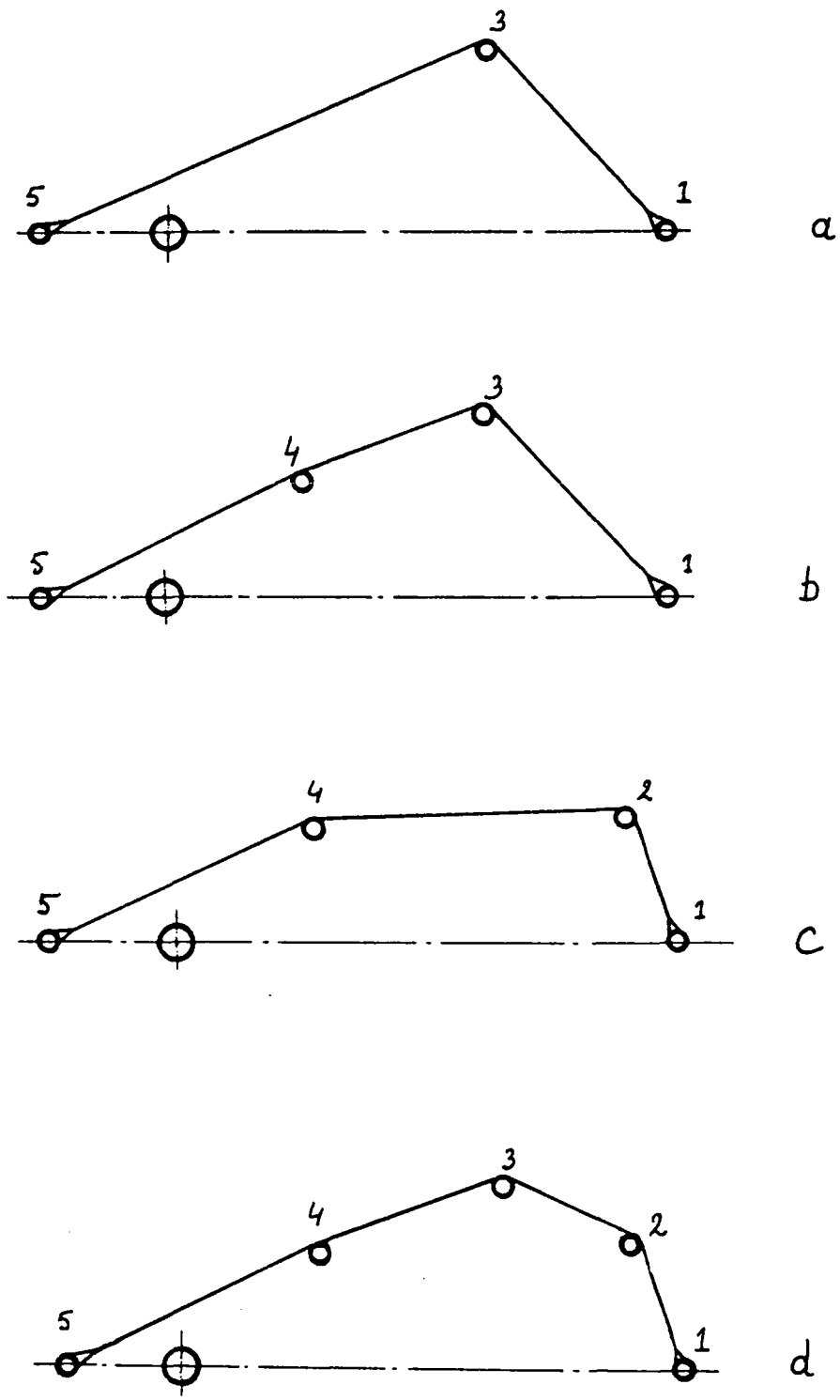

FIG. 9. Shapes of the tested configurations.

During a part of a revolution this area produces a large, negative torque.

b) Rotor with masts 1, 3, 4 and 5.
The performance is slightly better than in case a).
This rotor also oscillates initially.

c) Rotor with masts 1, 2, 4 and 5.
No oscillations are observed. The angular speed (without load) is much higher than in the cases a) and b). The negative torque in this case should originate from the sail area between masts 1 and 2, but for those wind directions in which this torque is negative, the other rotor half produces a positive torque of about the same magnitude.

d) Rotor with 5 masts.
The performance is now slightly better than in case c).

The above mentioned results were obtained in windspeeds of about 11 m/sec. The configurations a) and b) are obviously bad. No further measurements have been done on these configurations.

There is only a little difference between c) and d). For both these configurations a complete measurement has been executed. The resulting C_P-λ and C_Q-λ curves are plotted in Fig. 10 to 15. The curves are based on the computed data, mentioned in table 1 and 2 in Appendix III.

The influence of endplates

The endplates consist of bord, consolidated by latches. We tested three forms of these plates, as shown in Fig. 16. In all three cases we did a complete measurement. The results are shown in Fig. 17 to 24 and in tables 3, 4 and 5 in Appendix III.

It is clear from Fig. 24 that there is an optimum in the size of the endplates. This is due to the competition of two effects. First, by increasing the size of the endplates, the tip losses of the Savonius sails will be reduced. But at the same time the resistance of these endplates will increase, causing an extra power loss.

An unexpected result can be seen in Fig. 20. The starting torque of the sail Savonius decreases with increasing endplates.

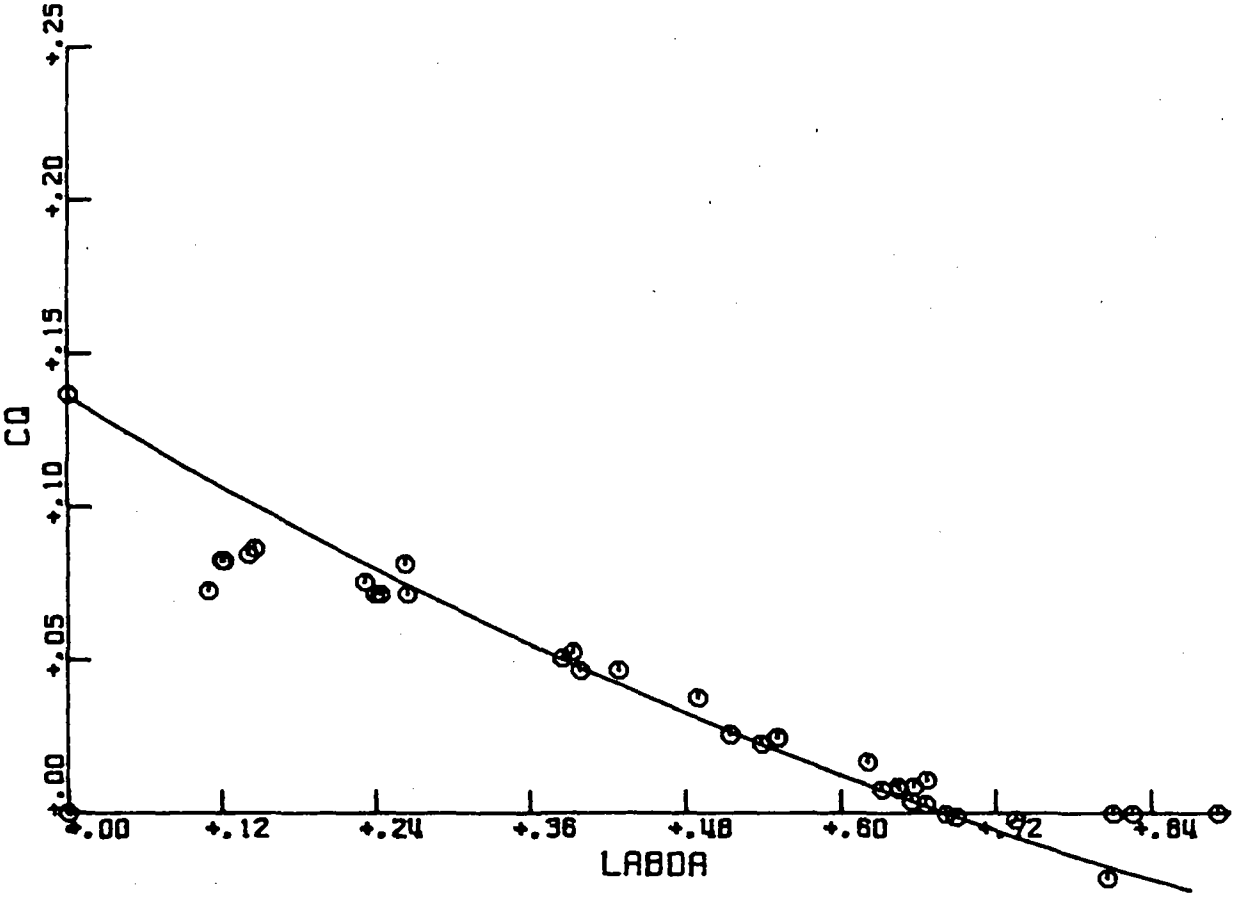

FIG. 10. $C_Q-\lambda$ curve, blade shape conform Fig. 9c.

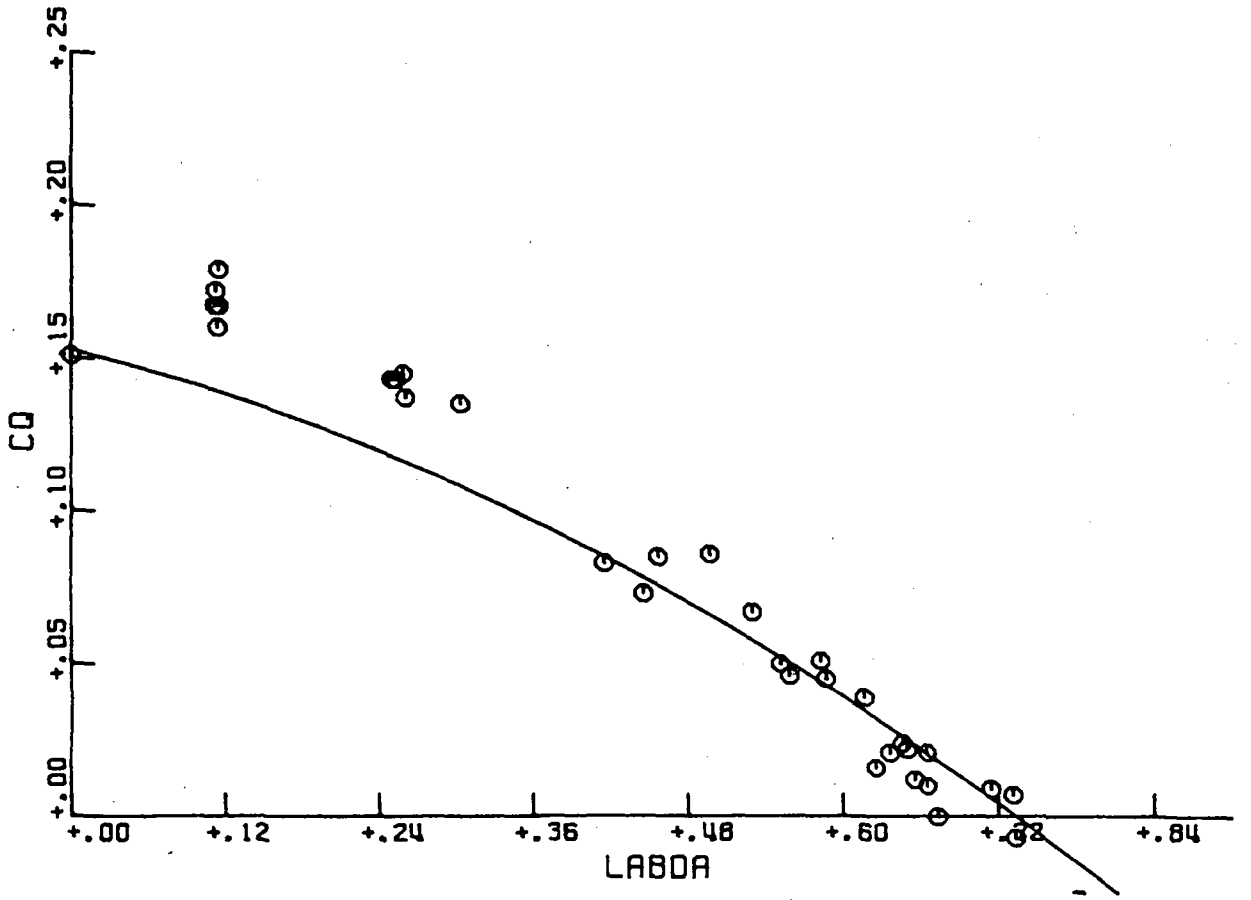

FIG. 11. $C_Q-\lambda$ curve, blade shape conform Fig. 9d.

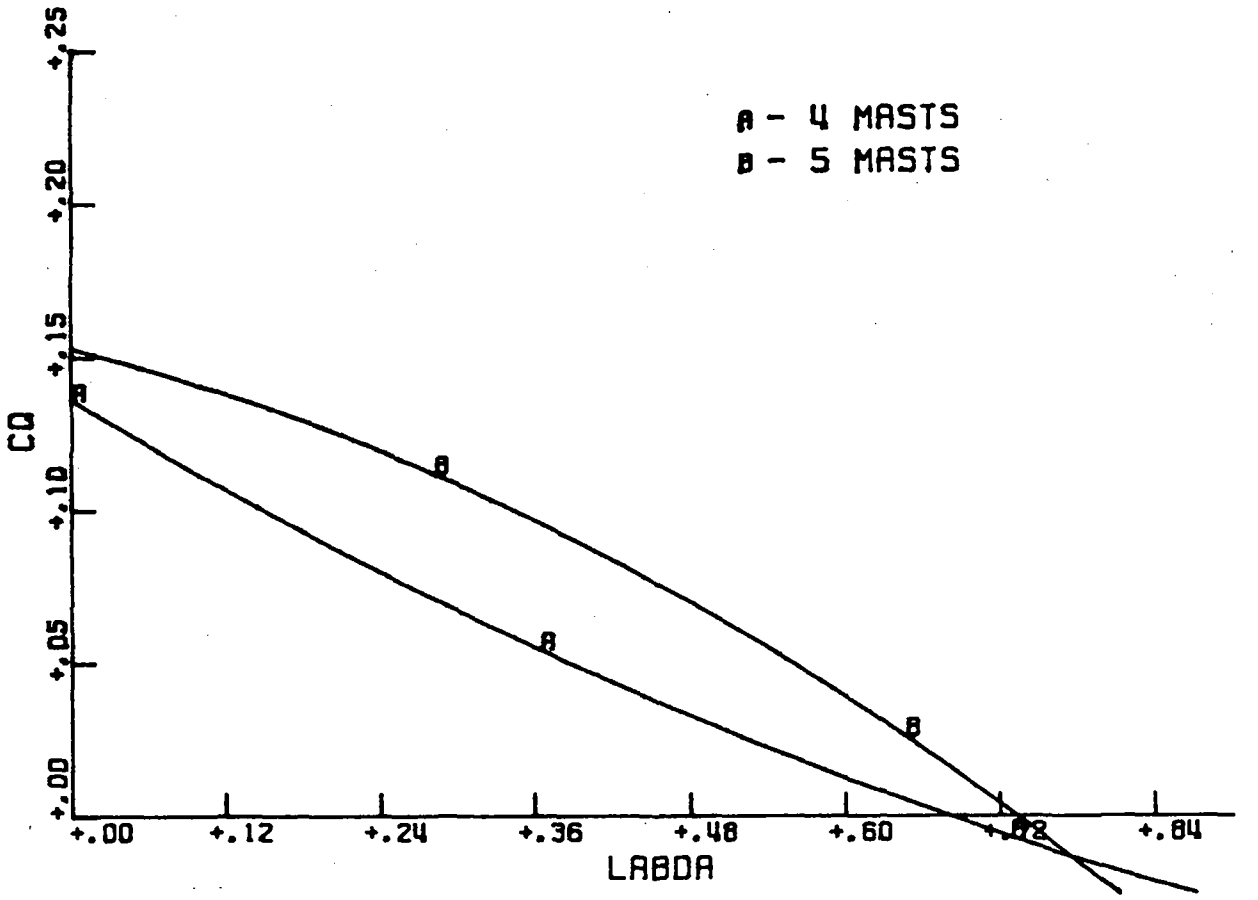

FIG. 12. $C_Q - \lambda$ curve, combination of Fig. 10 and 11.

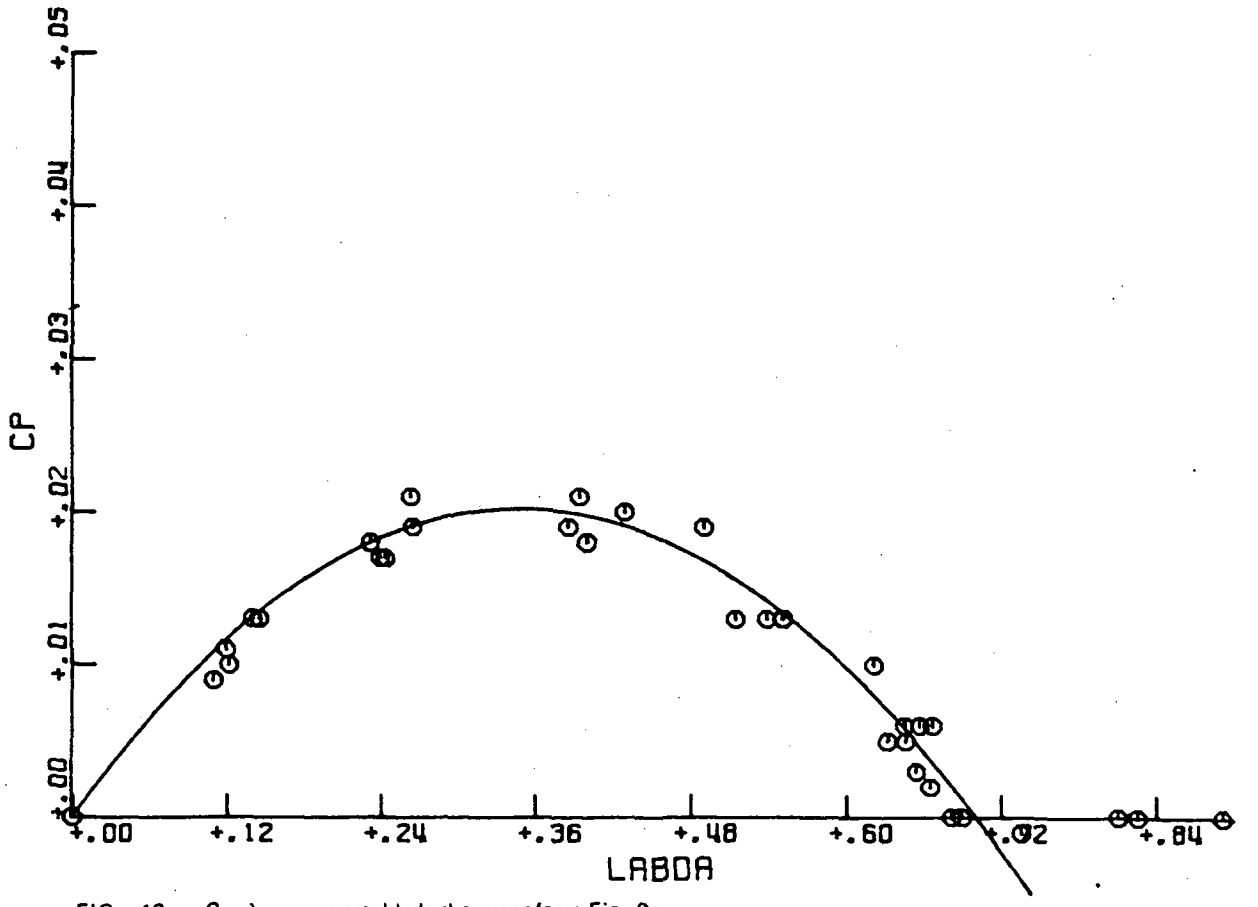

FIG. 13. $C_P - \lambda$ curve, blade shape conform Fig. 9c.

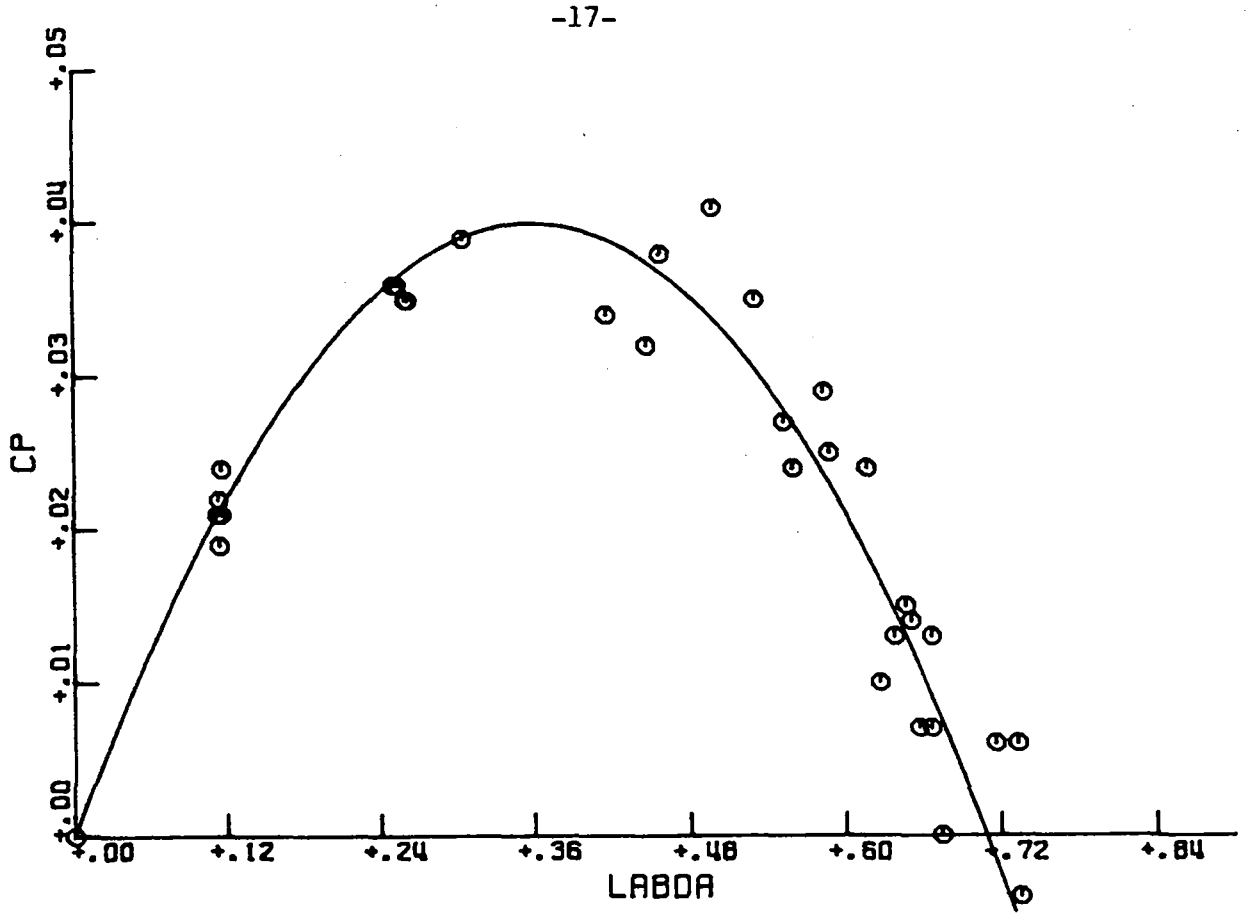

FIG. 14. $C_p-\lambda$ curve, blade shape conform Fig. 9d.

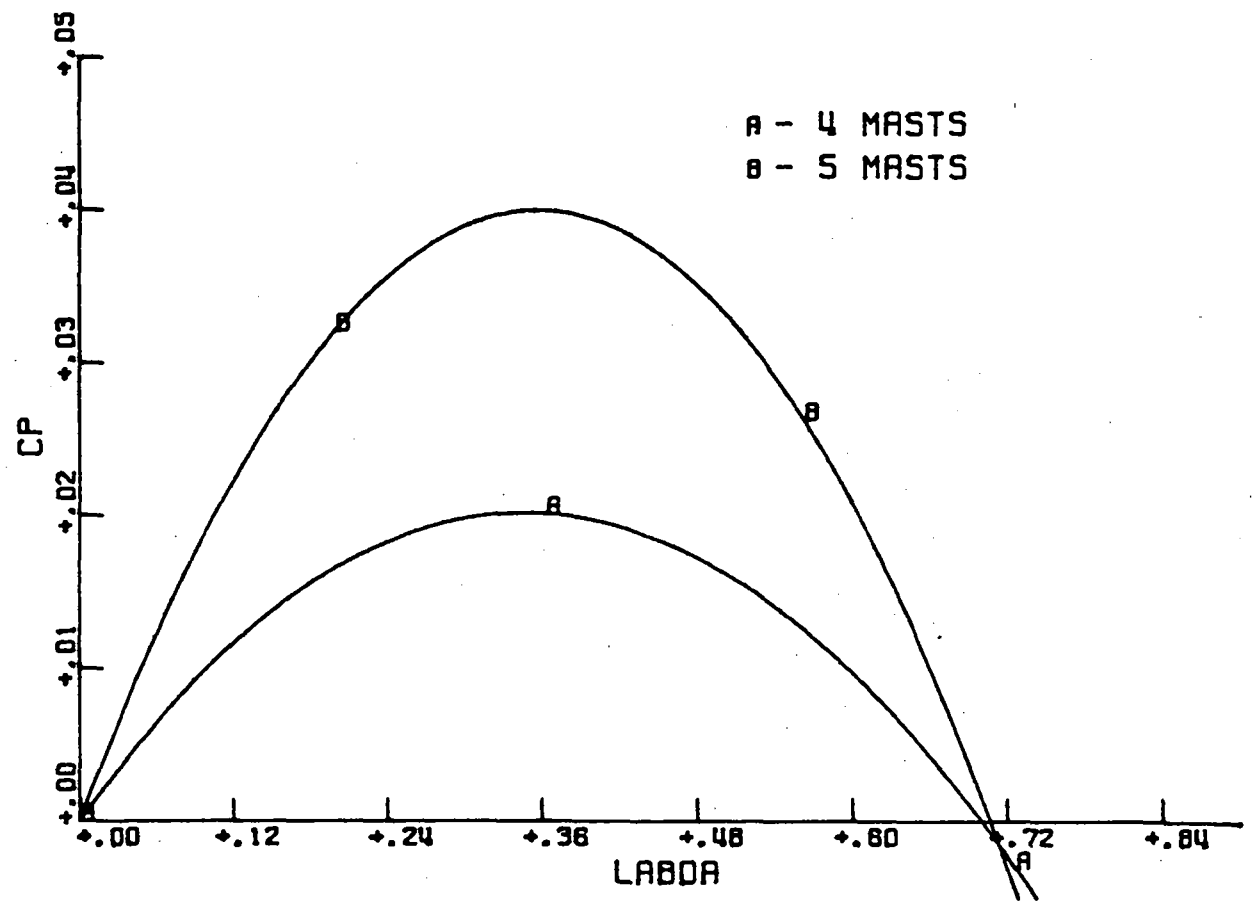

FIG. 15. $C_p-\lambda$ curve, combination of Fig. 13 and 14.

5. THE CONSTRUCTION OF A WOODEN SAVONIUS ROTOR

The performance of a Savonius rotor is not as good as a horizontal axis wind turbine. Wind tunnel tests indicate a maximum obtainable power coefficient varying between 0.2 and 0.25, while a horizontal axis wind turbine reaches to 0.40 and more. The advantage of a Savonius rotor is his rather simple construction. It is a slow rotating device and his performance is independent of the wind direction.

To see how a really simple design would perform we have built a Savonius rotor mainly using wood, sails and ropes. During the tests some alterations were carried out.

In this description we will distinguish three components:

a. the rotor
b. the bearings
c. the frame

In our case the rotor drives a membrane pump. This will be described in part d of this chapter.

a. The rotor

A single rotor has the disadvantage of a varying torque. Particularly in starting this can be tedious. To overcome this problem we constructed a rotor consisting of two parts: two rotors above each other, the upper one turned 90^{o} with regard to the lower one. Variation in torque is considerably reduced now.

The dimensions of one rotor half are (Fig. 25):

Diameter	d = 2.2 m
Width of one blade	a = 1.5 m
Gap width	s = .8 m
Diameter axis	b = .12 - .15 m
Height of a sail	h = 2.0 m

With these data the next ratios are found (cf. chapter 2):

1. Gap width-diameter ratio.
   s/d=0.36. This is rather large, due to the thick axis.

2. Aspect ratio.
   h/d=0.9. This is rather small. A greater ratio is obtainable in two ways: by constructing a higher rotor or by diminishing the diameter. The length of the central axis is limited by the available trees, this limits the height of the mill to about 7m. In diminishing the diameter we would get a rather small swept area and thus less power.
3. Central axis-gap width ratio.
   b/s=0.16. A normal ratio. The gap width is choosen relative to the axis diameter to avoid a blockage of this gap by the axis.

Dimensions of the complete rotor (Fig. 25):

Rotor height	H = 4.5 m	(sails + wood construction)
Length of axis	L = 6.3 m	
Weight	about 70 kg	

The sail shape is the same as on our teststand (see Annex I).

Initially all wooden parts of the rotor were held together by ropes (Fig. 26, 27). This gave difficulties. Ropes shrink in wet weather and stretch again in dry weather, thus causing all connections to loosen. To overcome this problem we tried two solutions. The first is applied to the upper rotor half. All connections are now masts with bolts (M6). The second method, applied to the lower rotor half maintains the ropes. A hole is drilled through layer and mast (diameter 10 mm). This hole is filled thereafter with a beech pin. Both methods gave satisfying results.

The rotor parts are attached to the central axis by a wedge and a groove (see Fig. 27). This attachment has proven to be a good one.

Reefing and hoisting can be done by one man. Reefing one rotor half will take about ten minutes, hoisting about twenty minutes. A man can stand in the rotor. The rotor has been operated in windspeeds up to 15 m/sec. When higher windspeeds were expected we always reefed the upper rotor half. The lower half never is reefed. After about one year of operation one of the lower sails broke down in a wind of about 25 m/sec. The sail could be repaired easily. (Windspeed is measured on a height of 4m, the centre of the complete rotor is 3.5 m above ground level).

b. The bearings

The bearings are made of wood. We used oak and elm. The lower bearing is the most crucial part of the mill. The rotor stands on it and it should withstand side-forces. Our construction is shown in fig. 28. On the axis we attached a ball (elm, diameter 0.23 m). This ball stands on a board of oak and is held in place by four blocks (oak). All these wooden parts are heated in oil for some days[16]. Our experience during the last year learns, that oil-soaking is a good way to conserve the wood. However, additional greasing is necessary.

The bottom of the ball is cone-shaped. The oak board under this ball has been replaced a few times. After three to four months turning, the ball has drilled its way through the oak board. (Thickness about 10 mm). We finally replaced the board by a sheet of steel (3 mm).

The friction between ball and blocks caused by side forces, is rather large, much larger than between the ball and the pieces of wood or steel under it. This friction causes considerable loss in torque. Partly this is due to the large diameter of the ball.

We have used a bearing of the same shape, but other dimensions and materials, in another vertical axis rotor. In that case the wear and tear is much less, and so are the friction losses. The materials and dimentions are:

ball	: akulon, diameter 24 mm
house	: cilinder of brass
rotor weight	: about 30 kg.

The upper bearing of the wooden Savonius consists of a wooden piece in the form of a cask, fastened on the top of the central axis (Fig. 29). This cask is held in place by a cross, which is a part of the frame.

c. The frame

The frame (Fig. 25, 29) consists of 4 poles. Each pole is held upright by three ropes. The tips of these poles are connected by a cross, which itself is a part of the upper bearing of the rotor.

The Savonius rotor is built in the following order:

1. The rotor is built, horizontally at ground level.
2. The cross is made.
3. Three piles are set up.

4. The cross is hoisted up high, but not yet fastened to the poles.
5. The rotor is set up (Fig. 29).
6. The cross is sunk a little, so that the top of the central axis goes through the hole.
7. The fourth pole is set up.
8. The cross is fastened to the 4 poles.
9. The ropes on the poles are adjusted so that the central axis stands vertically.

ad. 7. This attachment was initially done by ropes only. The cross will sink then, not fast, but steady. These ropes are later on replaced by bolts (M10).

d. The pump

The rotor drives a membrane pump. We used a commercially available pump. It is driven by a belt (Fig. 30). The pump is mounted on two piles (wood, pine) and hangs on the belt. The two belts stand at an angle of about 45 degrees. With this construction it is not necessary that the axis is straight. The behaviour of this transmission is satisfactory. The only difficulty is the rather great side-force in the lower bearing of the Savonius mill caused by the hanging pump.

The pully on the rotor axis is made of elm, diameter 0.2 m, those on the pump of afzelia, diameter 0.4 m.

e. The performance

No precise measurements have been carried out to determine the performance characteristics of the wooden Savonius rotor. A rough indication of its performance was obtained by measuring starting torque Q_{start} and speed at no load n(P=0) at a certain windspeed.

At 5m/sec: $Q_{start,max} = 40$ Nm
$Q_{start,\ average} = 25$ Nm
Rotorspeed (P=0)= 20 r.p.m.

Using the data mentioned in 5.a and assuming a linear torque-speed curve the next results are obtained:

$C_{Q,\ start} = 0.2$
$\lambda\ (P=0) = 0.4\ (\rightarrow \lambda_o = 0.2)$
$C_{P,\ max} = 0.02.$

It is obvious that this kind of construction is not advisable for Savonius rotors.

6. DISCUSSION OF THE RESULTS

Theory

The theoretical analysis of the coupling of a windrotor to a (constant torque) reciprocating pump clearly demonstrates the low overall efficiency of such a combination. It stresses the need to apply pumps with a quadratic torque-speed characteristic to ensure an optimum matching with the windrotor.

Experiment

A Savonius rotor equipped with blades in the form of sails around a small number (5) of rods exhibits a rather poor performance. Its power coefficients are of the order of 0.07, i.e. half or one third of what is measured elsewhere.

Sails around rods are aerodynamically not the best way to approach the ideal shape of a Savonius blade. The even poorer results of a double Sail Savonius with (thicker) wooden rods confirm this conclusion.

Applications

The potential of Savonius rotors for waterpumping, in comparison with modern multiblade windrotors, largely depends on the possibility of using a cheap and reliable construction method. As their power coefficient is roughly half of that of a horizontal axis multiblade rotor, their cost per m^2 swept area must be less than half. Our approach with sails around masts turned out to be reliable (the wooden rotor has withstood several storms up to 25 m/sec with only the upper half reefed) but not cheap because of the low powercoefficients.

More promising seems Govinda Raju's (Bangalore) approach[14]. He used metal wires, tensioned between two circular endplates, to support the sails. At least one such a rotor operates a tyre pump in an Indian village. No power coefficients are known to us.

The application of Sail Savonius rotors thus seems restricted to areas where wood and cloth are easily available, but metals scarce and more difficult to handle. The advantage of a vertical axis could be further enhanced by the use of a low speed rotating pump, to be coupled directly to the rotor axis, and preferable with a quadratic torque speed characteristic.

7. REFERENCES

1. C.E. Carver, R.B. Mac Person — Experimental investigation of the use of a Savonius rotor as a power generating device. Wind Energy, Achievements and Potential, Symposium Sherbrook, Canada, May 1974.

2. P.L. Fraenkel — Food from windmills. Intermediate Technology Publications London, 1975.

3. S. Sivasegaram — Design Parameters affecting the performance of resistance type vertical axis windrotors; an experimental investigation. Wind Engineering, Vol. 1, No. 3, 1977, p. 207-217

4. P.N. Shankar — The effects of geometry and Reynolds number on Savonius type rotors, National Aeronautical Laboratory, Bangalore, February 1976.

5. B.G. Newman — Measurements on a Savonius rotor with variable gap. Wind energy, Achievements and Potential, Symposium Sherbrook, Canada, May 1974.

6. G. Collins, R.J. Simpson — Tilting of windmills. Electronic and Power, June 1976, p. 347-351.

7. S. Blake — Savonius Rotor Wind Turbines. Wind Power Digest, ,1976, p. 25-27.

8. G. Bach — Untersuchungen über Savonius Rotoren und verwandte Stömungsmaschinen. Forschung auf dem Gebiete des Ingenieurswesens, 2, 1931, p. 218-231.

9. M.H. Simonds, A. Bodek — Performance test of a Savonius Rotor, Technical Report No. T10, Jan. 1964. Brace Research Institute, Quebec.

10. J.A.C. Kentfield — A magnified Savonius wind turbine with good low velocity-ratio torque characteristics. Wind Energy, Achievements and Potential, Symposium Sherbrook, Canada, May 1974.

11. E. Barnhart — Savonius Rotor. Journal of the New Achievements, No. 3, 1976, p. 27-29.

12. M.A. Hackleman, D.W. House — Wind and Windspinners. Earthmind, California, 1974.

13. J.F. Bonas (editors), W.N. Sullivan — Sandia Vertical Axis Wind Turbine Program, Technical Quarterly, Oct. 1975. SAND-76-0036.

14. S.P. Govinda Raju, K. Narahari Rao, R. Narasinka — Some windmill rotors suitable for use in a rural environment. Report 76 FM, India Institute of Science, Bangalore, Jan. 1976.

15. R.E. Wilson, P.B.S. Lissaman, S.N. Walker — Aerodynamic performance of windturbines, Oregon State University, June 1976.

16. J. Collett — Oil soaked wood bearings. Intermediate Technology Publications, London 1976.

17. B.F. Blackwell, R.E. Sheldahl, L.V. Feltz — Windtunnel performance Data for Two- and Three-Bucket Savonius Rotors. Sandia Laboratories, Albuquerque, June 1977. SAND-76-0131.

18. - — How to construct a cheap windmachine for pumping water. Brace Research Institute, McGill University, Quebec, February 1973.

ANNEX I THE TESTSTAND

When starting the activities on Savonius rotors we had a test stand available from experiments on a Chinese windmill. With a few modifications this teststand was used to test the sail Savonius. In this annex we will give a description of the Savonius teststand (Fig. 31).

The rotor rotates above the platform, in a steelframe. Underneath this platform is a cabin in which the measurement instruments are placed. The frame is schematically drawn in Fig. 32.

The rotor consists of an axis with an upper and lower circular frame, shown in Fig. 33. The whole is a strong and heavy construction, (total weight about 340 kg). The sail shape is chosen to be an approximation of Bach's[8] non-circular rotor form (Fig. 7). We tried to reach an acceptable approximation by means of 5 masts (Fig. 34). Mast 1, 2, 3 and 4 are fixed to upper and lower rotor part. The sail is attached to mast 1, pulled around mast 2, 3 and 4 and attached again to mast 5. This latter mast is fastened to the rotor by means of ropes. In this way the sail can be tightened and also easily reefed. The height of the sails is 1.80 m, the distance between upper and lower rotor 2.00 m.

The endplates are made of board, consolidated by latches (Fig. 16). Each endplate consists of two halves, fastened to each other by ropes. The under plate lies upon the lower rotor part, fastened with ropes. The upper plate hangs on the upper rotor part at a distance of about 0.2 m. The distance between the endplates is 1.80 m. (The sail is fastened to the plates by ropes).

The rotor axis goes through the platform into the cabin. The inside of the cabin is schematically drawn in Fig. 35. Going downwards on the central axis we see first a brake. This brake is operated manually. Then follows a torque measuring axis (Hottinger-Baldwin, type T2, maximum 200 Nm), a gear box and a electromotor with an eddy current coupling. The angular speed of the rotor can be controlled by regulating motor and coupling. The motor can rotate in two directions or the axis can be fixed to its housing. The torque trasferred to or from the rotor can be controlled by the eddy current coupling. The gear ratio is 1:21, in two stages, by means of timing belts. The rotational speed is measured by a tachometer, mounted on the eddy current coupling.

An electronic interface transforms the tachometer signal into two output signals. The tachometer gives a 5 phase A.C. current. This is changed into a series of pulses, having a block form, levels 0 and 5 V. The frequency is a linear function of the angular speed. The other output is a D.C. voltage, obtained by integration of the pulse train. This signal also is a linear function of the angular speed.

By means of an electronic regulator the eddy current coupling can be regulated in such a way, that the rotor operates at a constant rotational speed or at a constant torque.

ANNEX II THE TESTPROCEDURE

The aim of the experiments is to determine C_P-λ and C_Q-λ curves. C_P, C_Q and λ are tied up by

$$C_P = \frac{P}{\frac{1}{2}\rho A V_\infty^3} = \frac{Q.\Omega}{\frac{1}{2}\rho A V_\infty^3}$$

$$C_Q = \frac{Q}{\frac{1}{2}\rho A R V_\infty^2}$$

$$\lambda = \frac{\Omega R}{V_\infty}$$

From the above formulae it can be seen that we have to measure three variables: torque (C_Q), angular speed of the rotor (Ω) and the wind velocity (V).

Determining C_P, C_Q and λ from these variables can be done in two ways.
1. At a certain moment take the value of the three variables, and determine C_P, C_Q and λ. This is only possible when at this moment the rotor operation is steady, i.e. a momentary constant angular speed, constant torque and constant wind speed.
Now there arise a series of difficulties:

a. There is some distance between the rotor and the anemometer (10m). The wind velocity at the rotor is different from the velocity at the anemometer. One way to obtain a good information about the wind velocity the rotor feels is measuring at some distance above and under the rotor, and determine a wind velocity from these two measurements. In our case it is impossible to measure the wind velocity under the rotor. Measuring only above the rotor gives a too high wind velocity.

b. Even in winds with constant direction and velocity, the torque of a Savonius rotor is not constant. It is known from the literature that torque varies considerable in one revolution.

Mainly for this last reason this method of determining C_P, C_Q and λ values is not suitable for us.

2. The second method goes as follows. We measure during some time the three variables. C_P, C_Q and λ are determined by taking the average.

We have used this second method. We can distinguish two stages in coming to our aim:

A. Data gathering

B. Data processing.

We will give now details about both parts of the process.

A. Data gathering

For the data gathering we use a microprocessor system (Fig. 36). The m.p. is developed in our laboratory. The used components are of the Motorola M 6800 family. The data are stored on a magnetic tape by means of a Facit 4203 cassette recorder.

The processor is capable in handling a number of signals. There are two digital input channels, which can accept pulse traines, and one analog input channel which can accept, by means of a multiplexer, up to eight analog signals. The m.p. system can be operated from a keyboard.
The program operates as follows:

1. After the system is reset we first can type text. All typed characters are stored on the tape.
2. Before starting a measurement we have to give the m.p. three parameters.
   a. The sampling period. During this time the pulses from the digital input channels are accumulated in two counters. At the end of the period the data of the counters are stored on the tape and the counters are reset. Sampling rate between 1 and 99 sec.
   b. The number of analog signals be scanned by the multiplexer. The multiplexer scans the channels once per sampling period. Each channel needs 2 sec. to be read. This time is necessary for the D.V.M., to reach his endvalue after being connected to an input channel. From this we can establish the minimum sampling period. This is $t = 1+2 * N$ sec, N = number of analog signals. Time is measured by the m.p. in seconds.
   c. The total measuring time. The m.p. stops after this time is up. After starting always one cyclus is carried out. The maximum time is 99999999 sec. (= 27.7777.77 hrs., 1157.4 days, = 3.17 years).

3. After these parameters are accepted by the m.p. system the measurement can be started. The processor then proceeds conform the given parameters.

We use only one analog channel: the torque. Sampling is done at the maximum rate so the sampling period is three seconds. A complete measurement is executed as follows:

1. Text is typed with some data: the configuration of the rotor, the kind of weather, etc.
2. The rotor is fixed to measure the starting torque. The parameters are given, total measuring time 600 sec., the measurement is started. 5 measurements are carried out with a fixed rotor at different angular position of the rotor, because of the dependency of the torque of this position.
3. The rotor is operated at constant rotational speed, with the electromotor fixed. Total measuring time is 1000 sec. This measurement is done at several speeds.
4. The rotor is operated at constant speed, el. motor turns in the same direction as the mill. We now can compensate the losses in the gearbox. A number of measurements are carried out, with different speeds, until we measure negative torques. It takes about three hours to execute a complete measurement.

B. Data processing

The data are worked up at the computer.

From sixty samples we calculate the mean of:

V_∞, V_∞^2, V_∞^3, Ω, Q and $P(=Q.\Omega)$.

$$\overline{V_\infty} = \frac{1}{60}\sum_{i=1}^{60} V_{i\infty} \; ; \quad \overline{V_\infty^2} = \frac{1}{60}\sum_{i=1}^{60} V_{i\infty}^2 \; ; \quad \overline{V_\infty^3} = \frac{1}{60}\sum_{i=1}^{60} V_{i\infty}^3$$

$$\overline{\Omega} = \frac{1}{60}\sum_{i=1}^{60} \Omega_i$$

$$\overline{Q} = \frac{1}{60}\sum_{i=1}^{60} Q_i$$

$$\overline{P} = \frac{1}{60}\sum_{i=1}^{60} Q_i \cdot \Omega_i$$

λ, C_P and C_Q are now calculated according to:

$$\lambda = \frac{\bar{\Omega} \cdot R}{\bar{V}_\infty}$$

$$C_Q = \frac{\bar{Q}}{\frac{1}{2} \rho A \bar{V}^2 R}$$

$$C_P = \frac{\bar{P}}{\frac{1}{2} \rho A . \bar{V}^3}$$

with : $\rho = 1.25 \text{ kg/m}^3$

$A = 4.32 \text{ m}^2$.

Due to the variations in wind and torque there exists a large variation in the so obtained points. A second part of the computer program now calculates a C_P-λ and a C_Q-λ curve from the calculated points. Every point is given a weight, proportional to the square of the inverse of the relative spreading in the wind velocity during the measurement period. The C_P-λ curve is approximated by a third order polynomial and the C_Q-λ curve by a second order one.

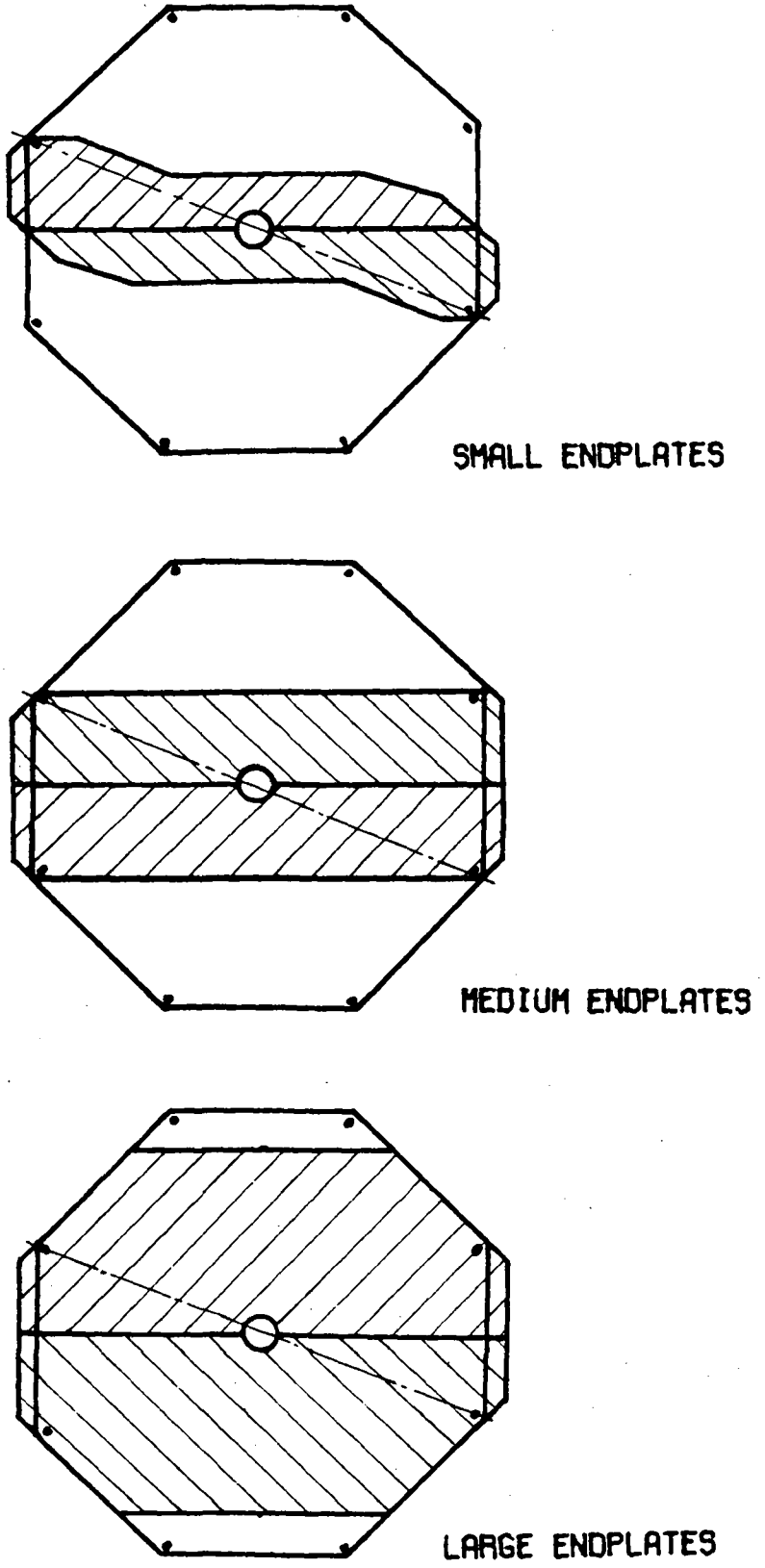

FIG. 16. Shape of the endplates.

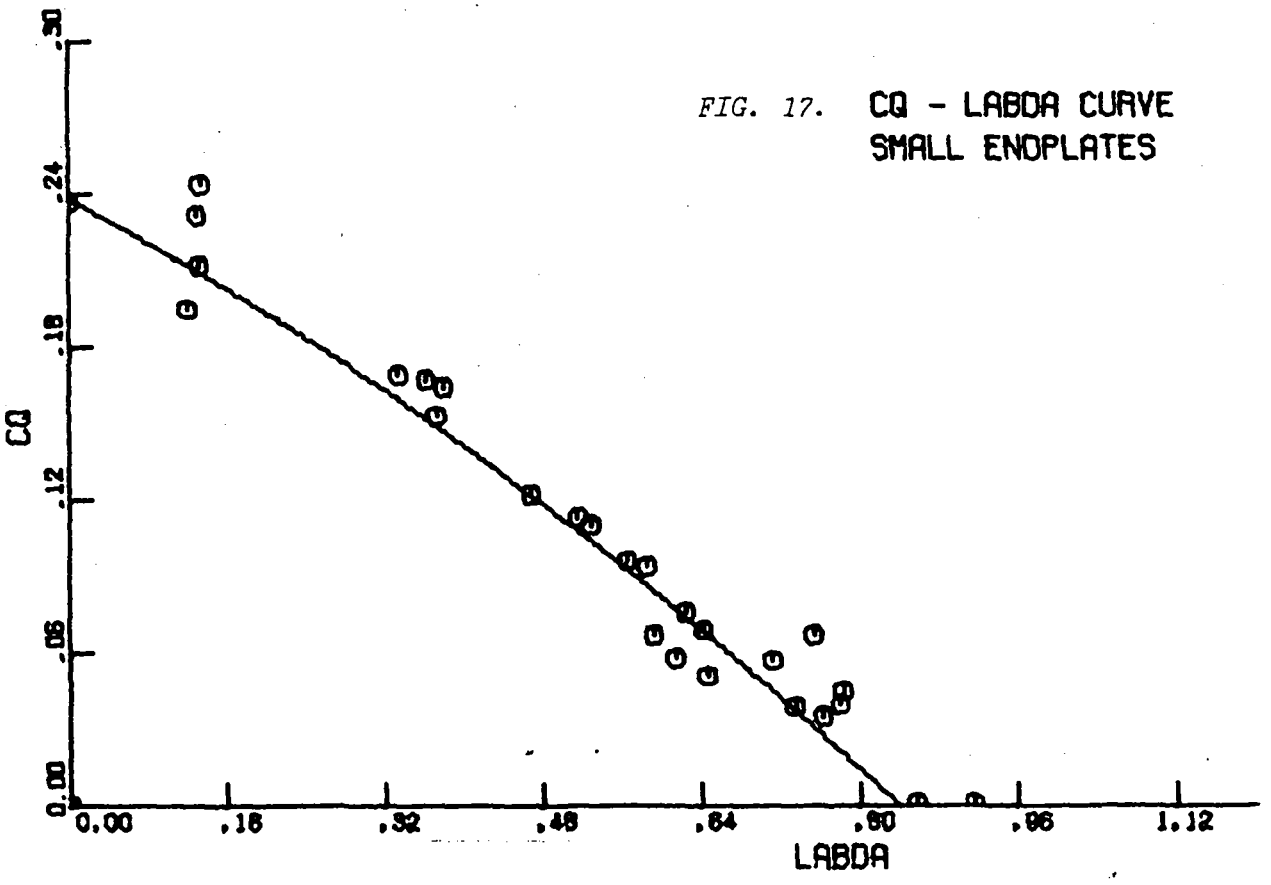

FIG. 17. CQ - LABDA CURVE
SMALL ENDPLATES

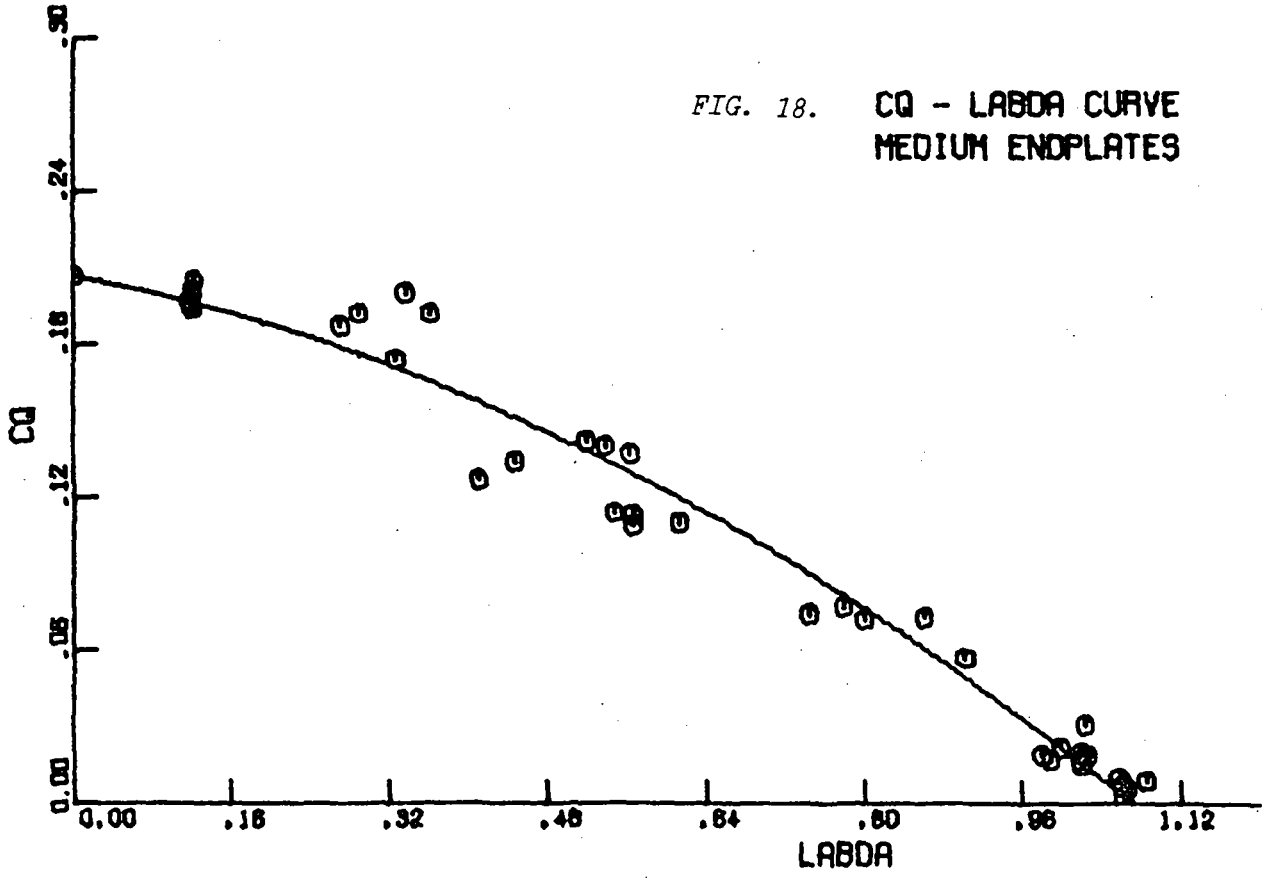

FIG. 18. CQ - LABDA CURVE
MEDIUM ENDPLATES

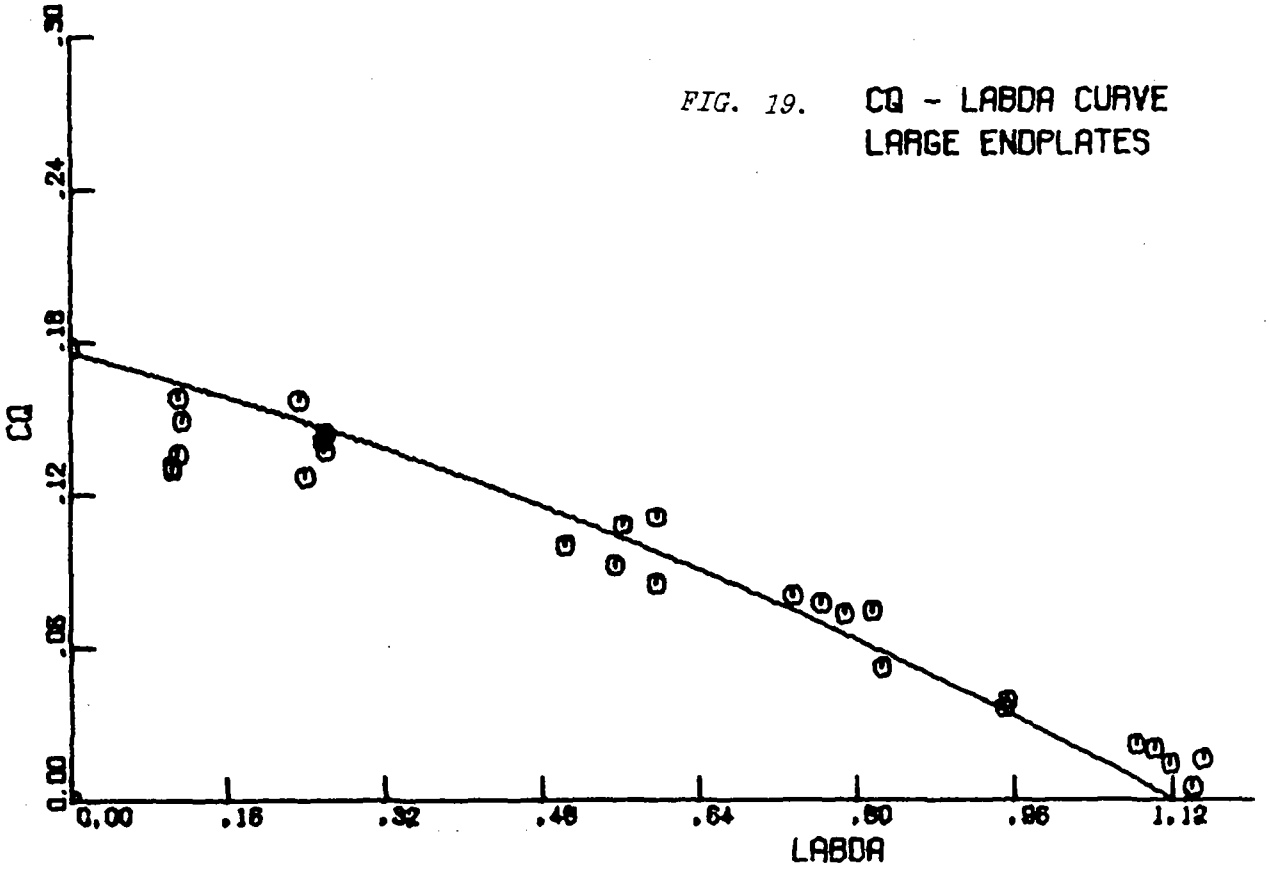

FIG. 19. CQ - LABDA CURVE
LARGE ENDPLATES

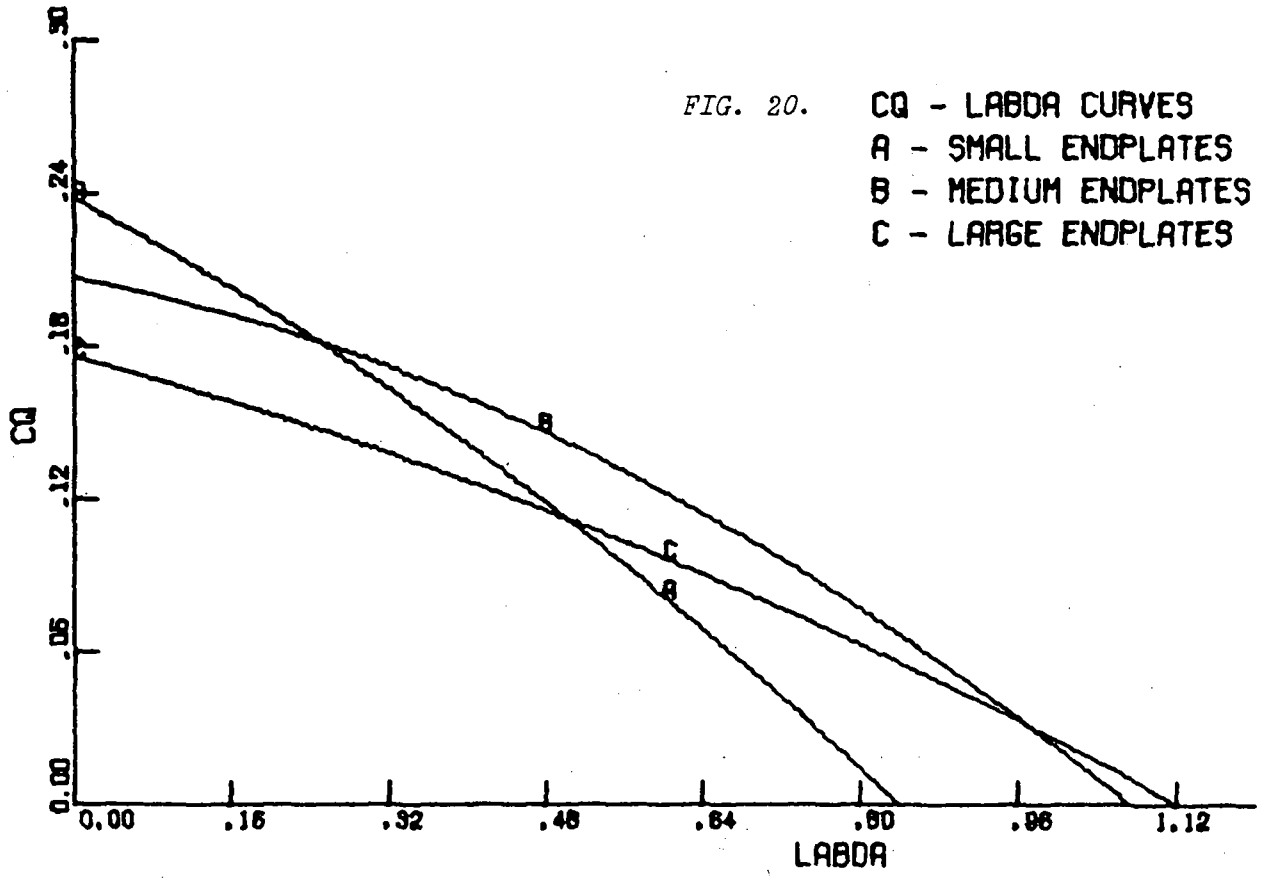

FIG. 20. CQ - LABDA CURVES
A - SMALL ENDPLATES
B - MEDIUM ENDPLATES
C - LARGE ENDPLATES

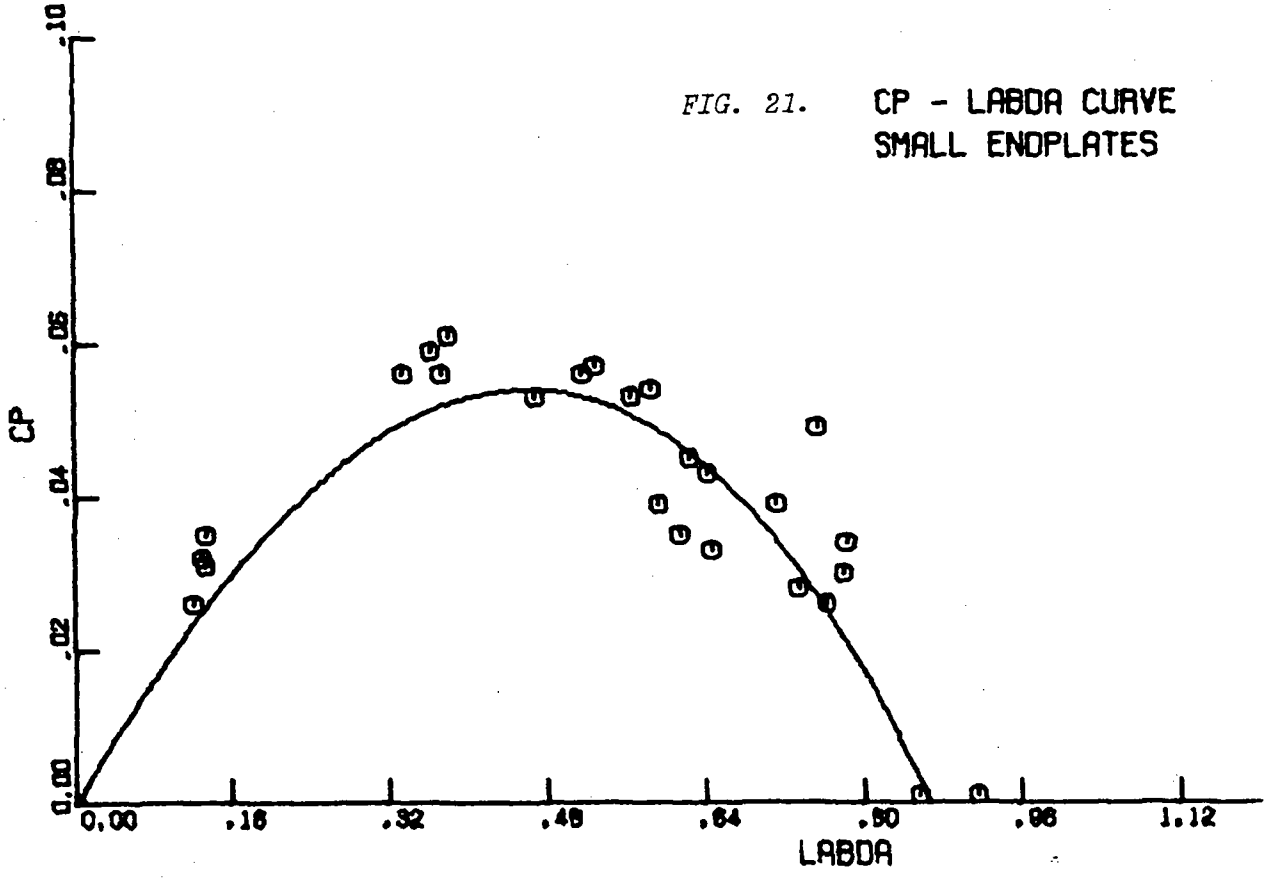

FIG. 21. CP - LABDA CURVE
SMALL ENDPLATES

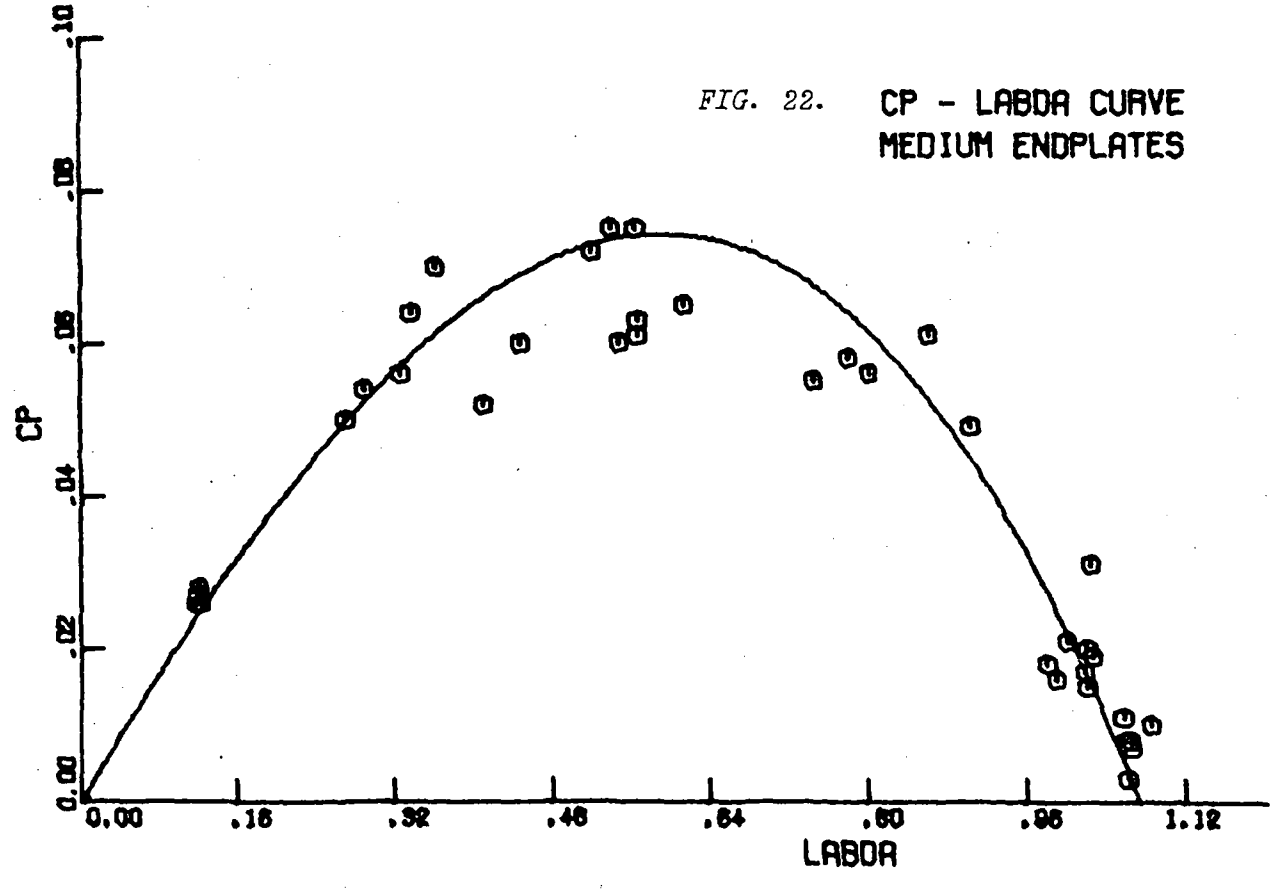

FIG. 22. CP - LABDA CURVE
MEDIUM ENDPLATES

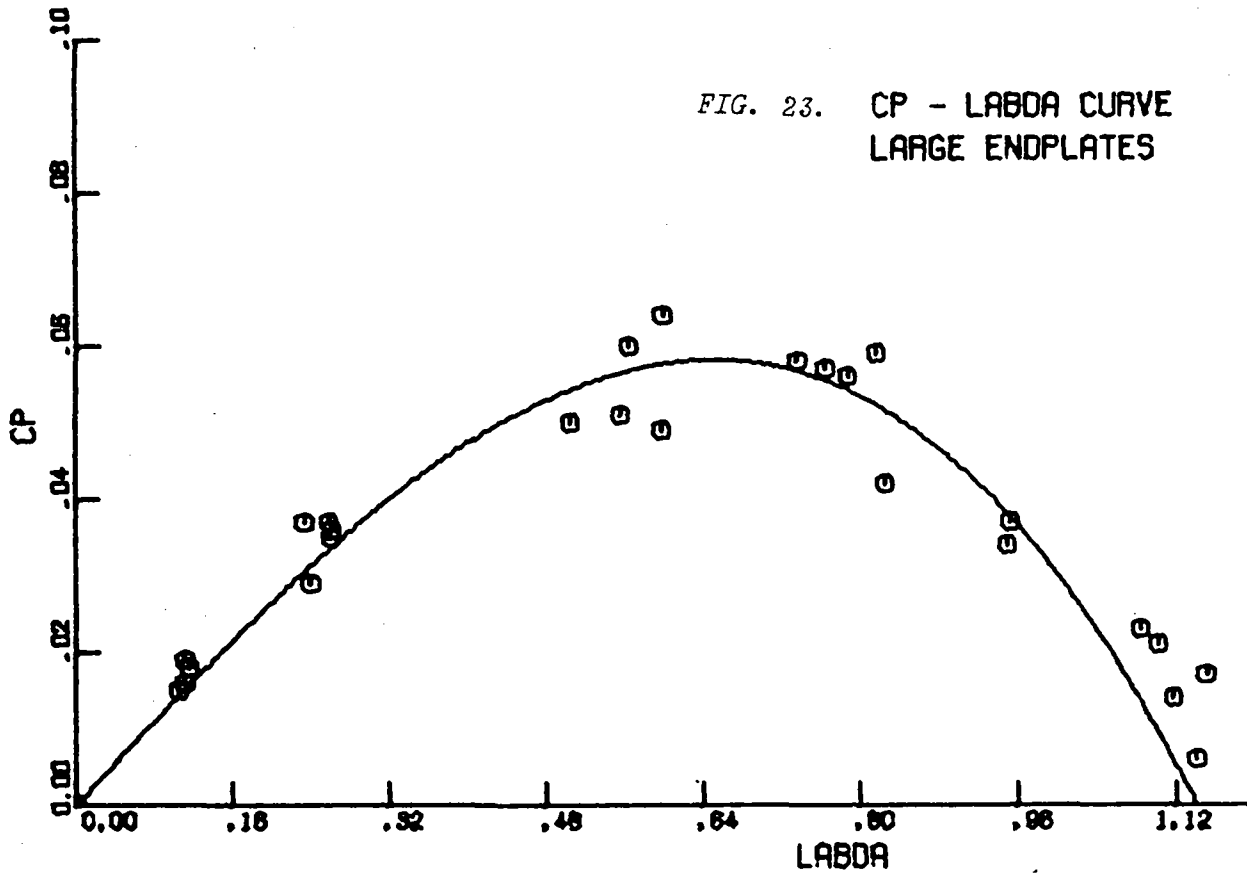

FIG. 23. CP - LABDA CURVE
LARGE ENDPLATES

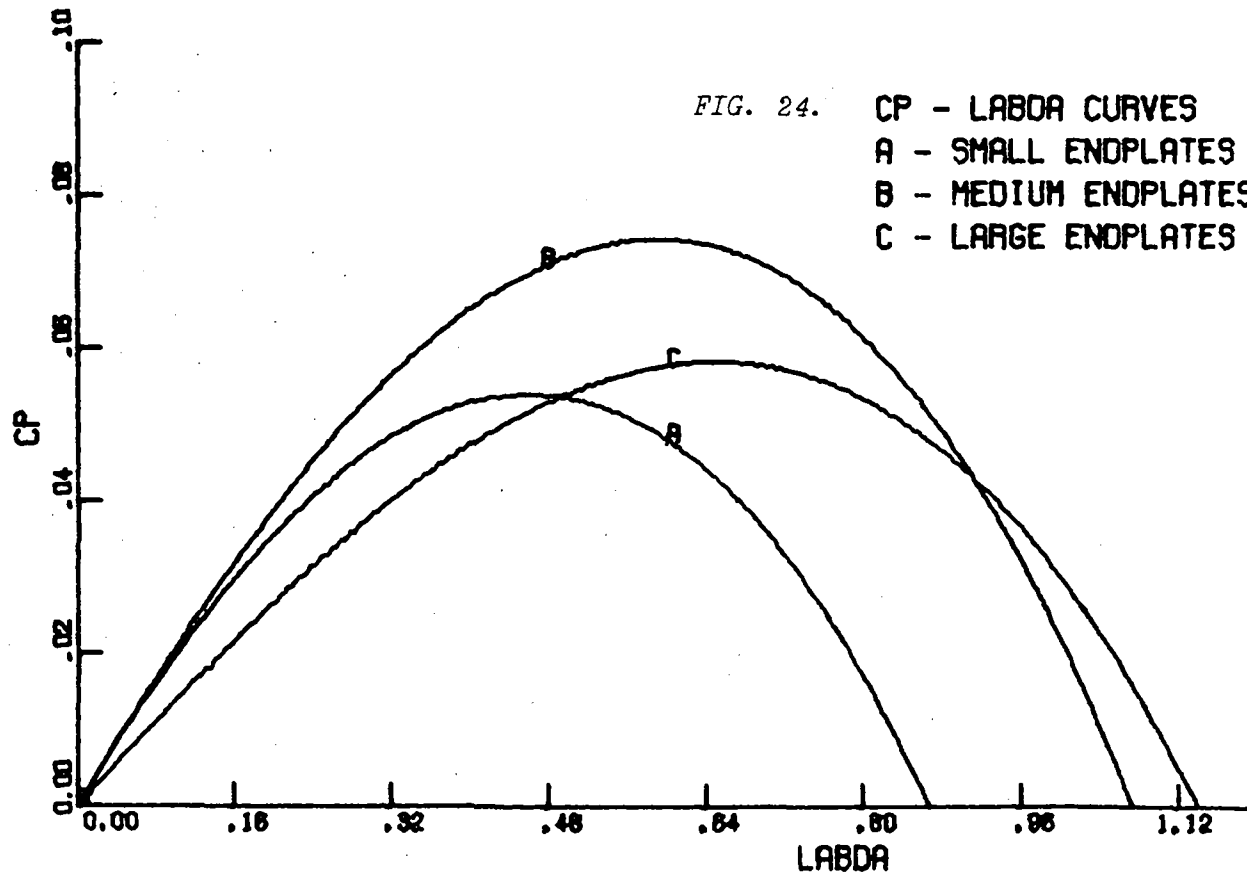

FIG. 24. CP - LABDA CURVES
A - SMALL ENDPLATES
B - MEDIUM ENDPLATES
C - LARGE ENDPLATES

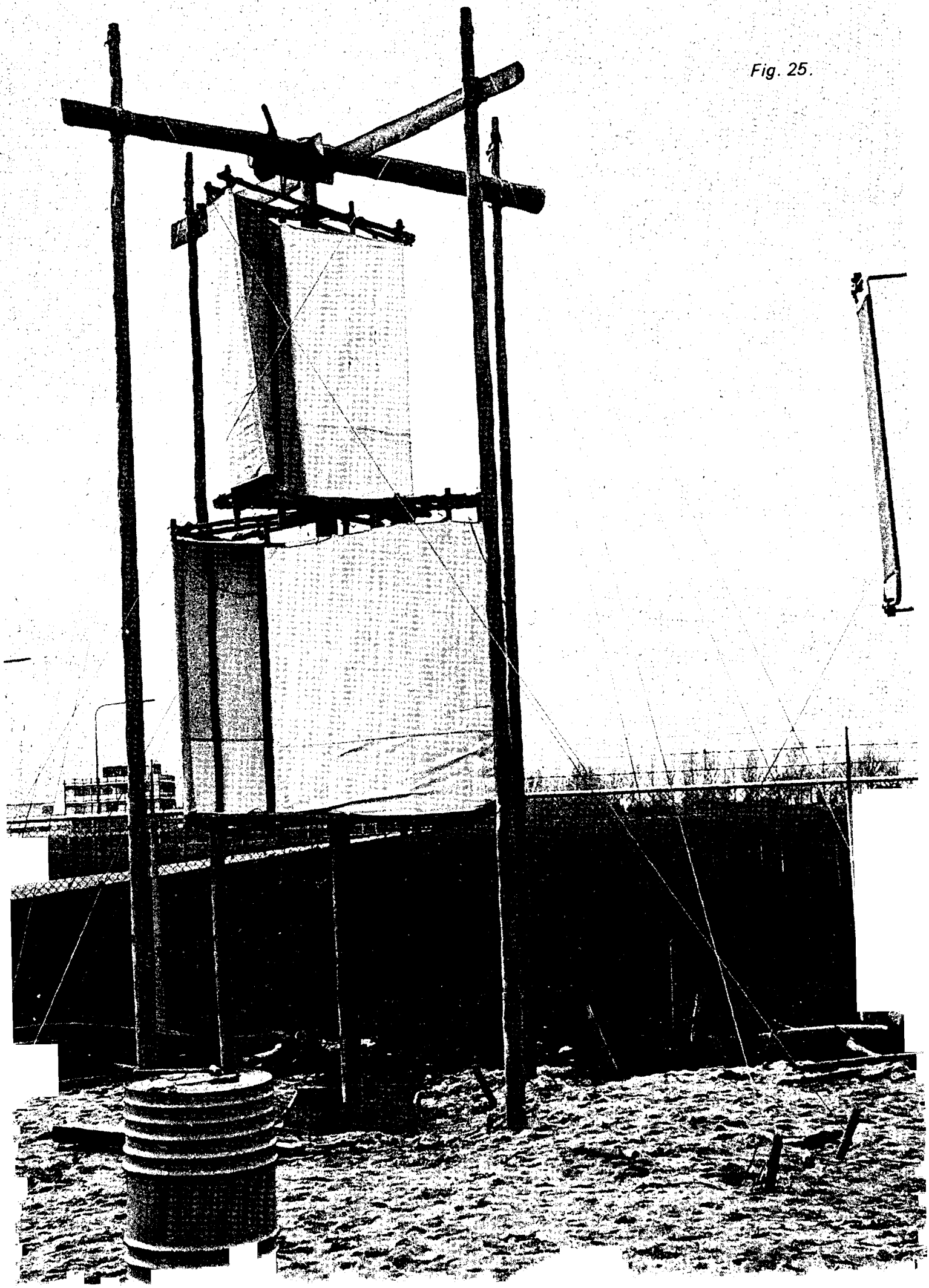

Fig. 25.

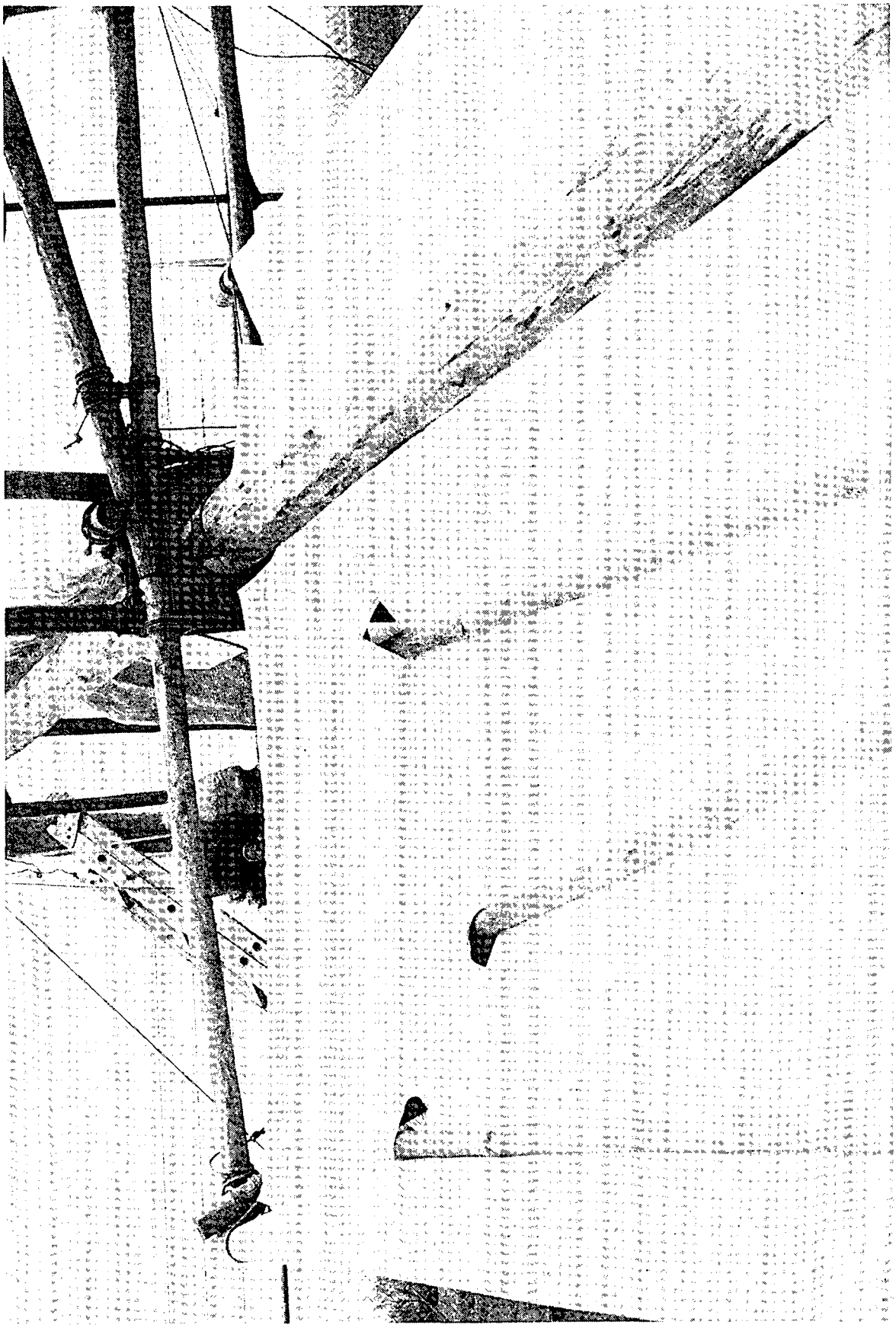

Fig. 26. Detail of the rotor in the construction phase.

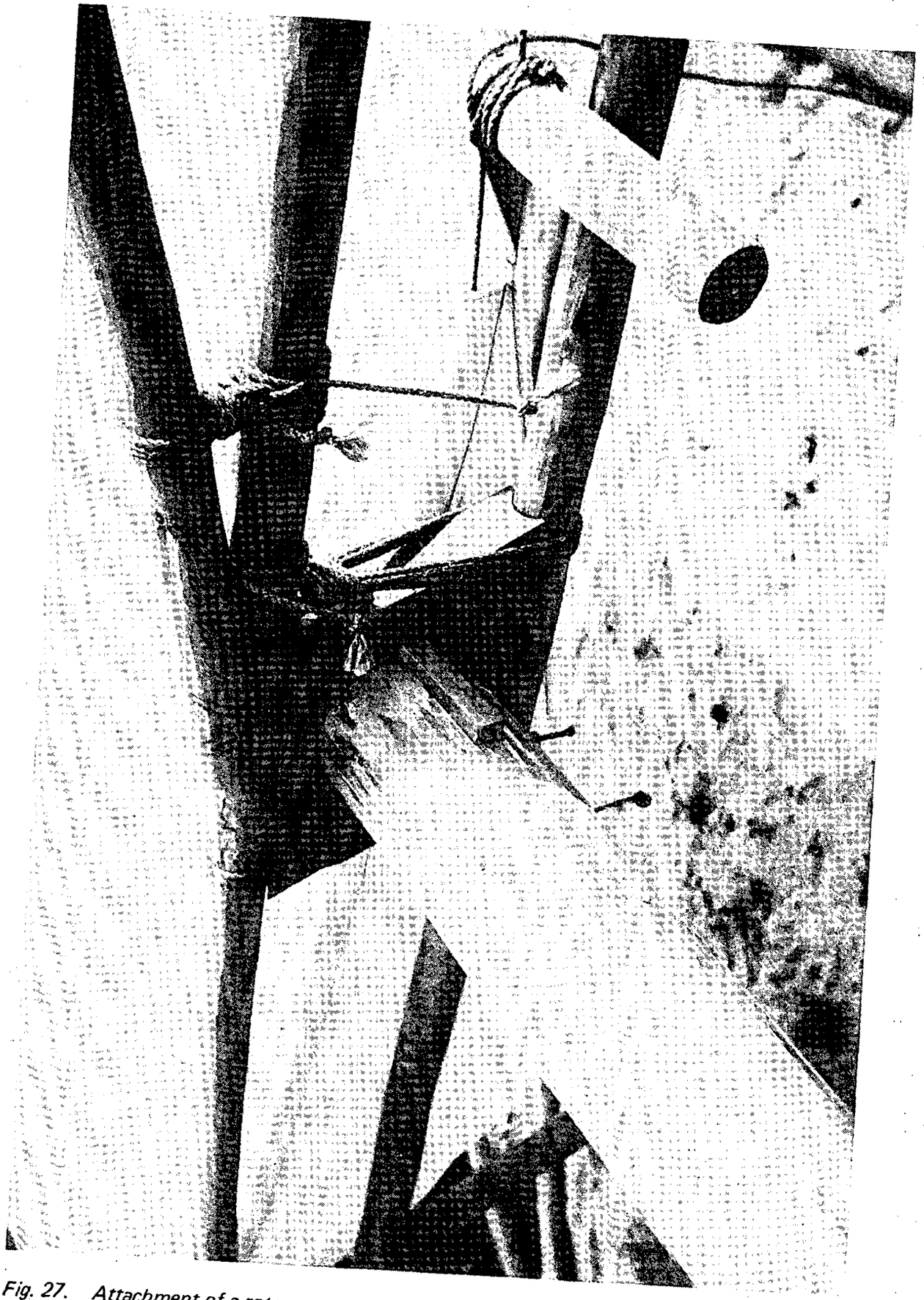

Fig. 27. Attachment of a rotor part to the axis.

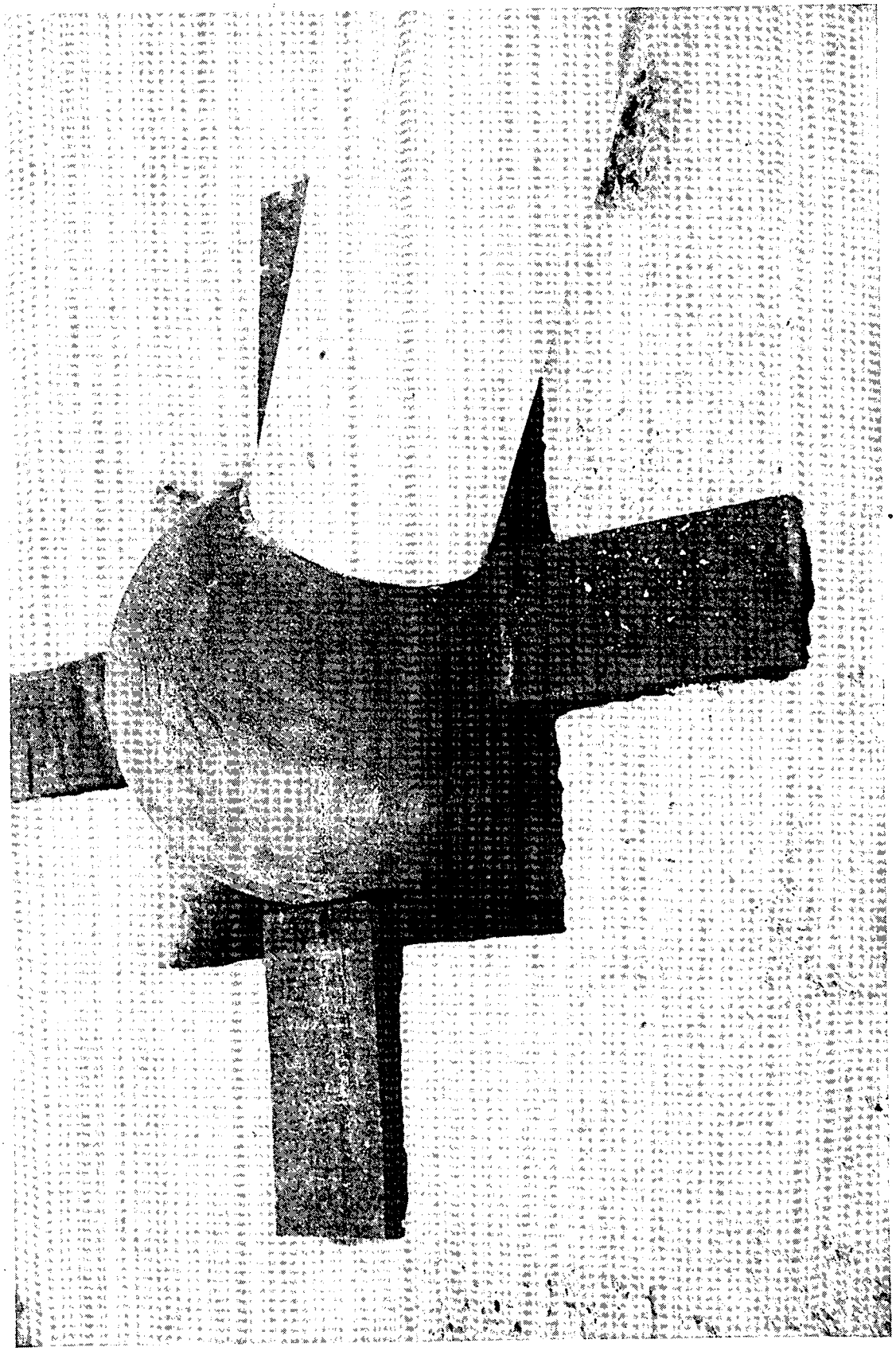

Fig. 28. Lower bearing, rotor not yet set upright.

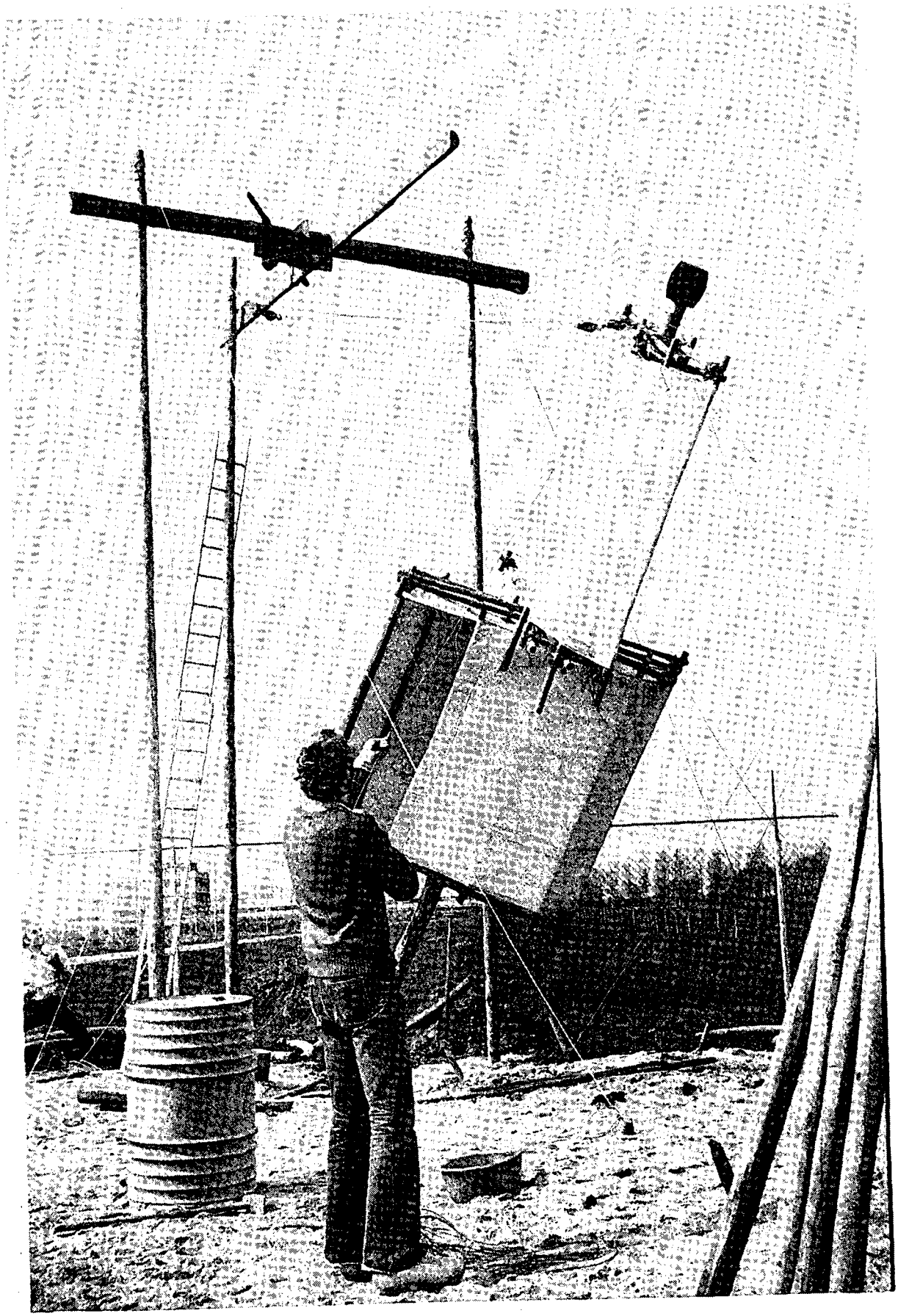

Fig. 29. The setting up of the rotor.

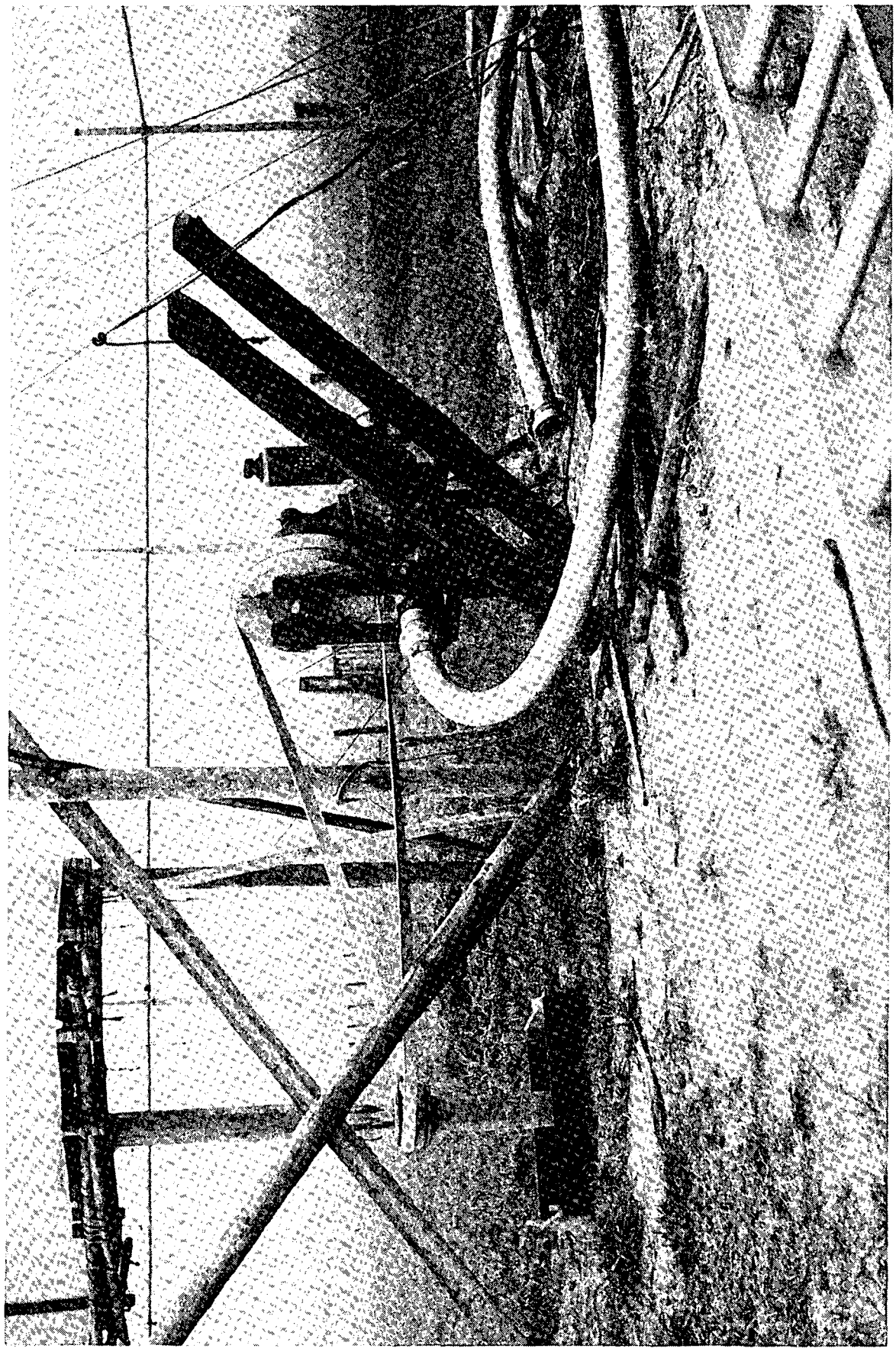

Fig. 30. Pump, hanging at the rotor axis.

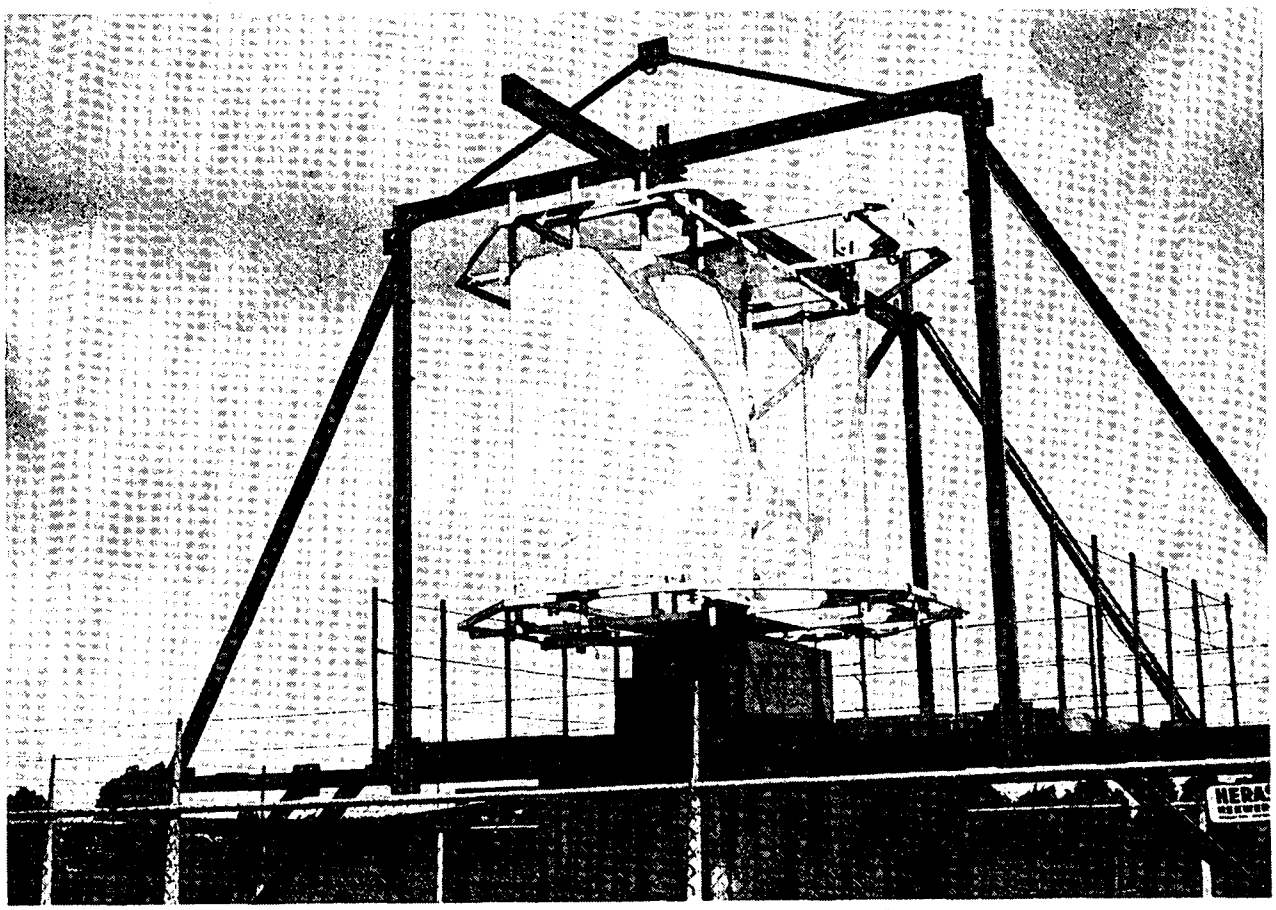

Fig. 31. The teststand equipped with a Savonius rotor with five masts per blade, but without endplates.

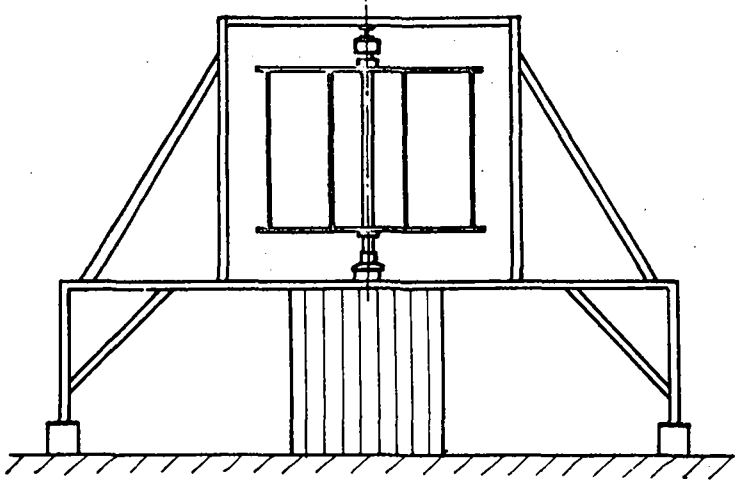

FIG. 32. The teststand, schematically.

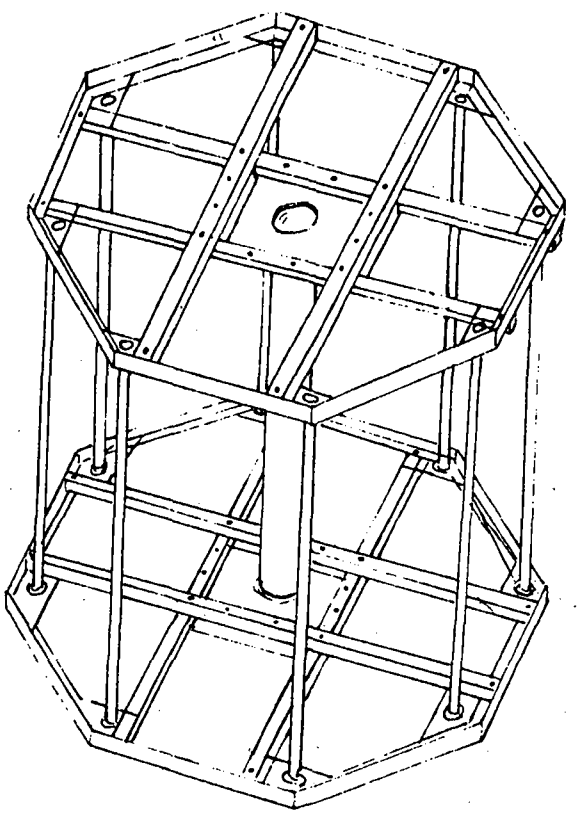

FIG. 33. The rotor of the teststand.

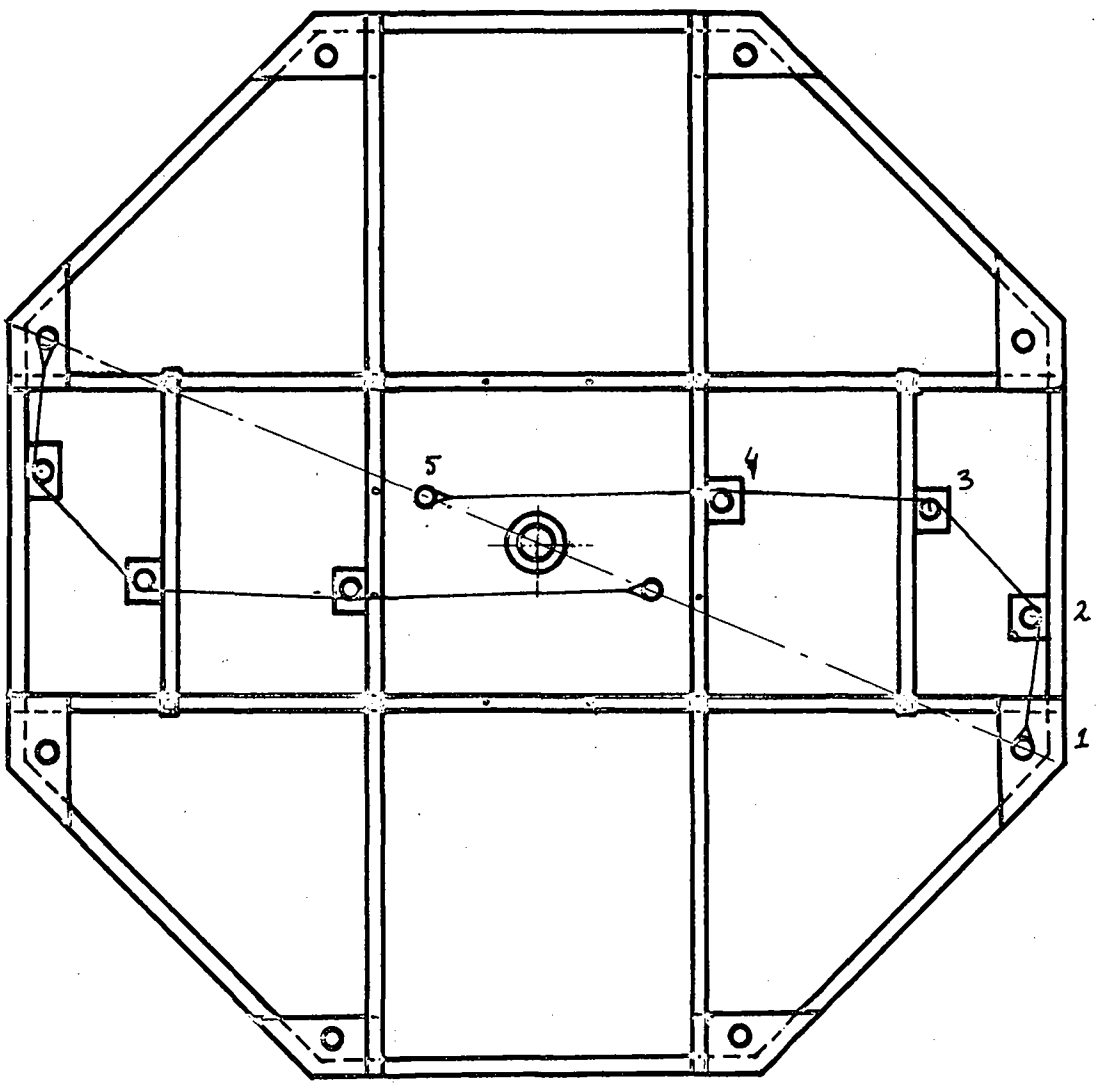

FIG. 34. Position of the mastst in the rotor.

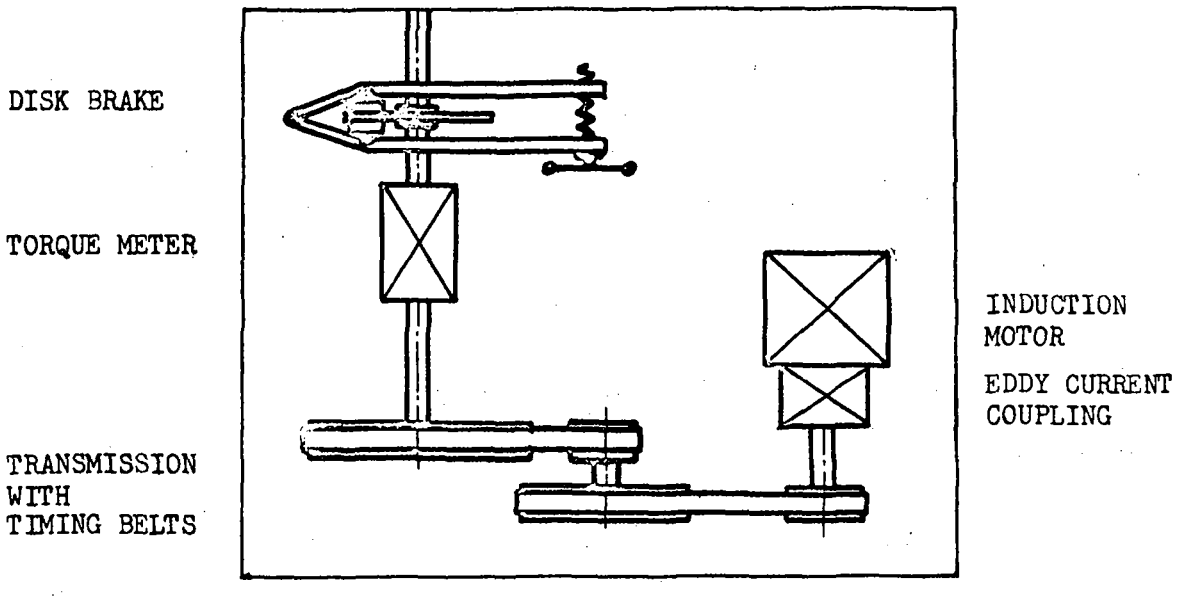

FIG. 35. The equipment inside the cabin beneath the rotor (schematically).

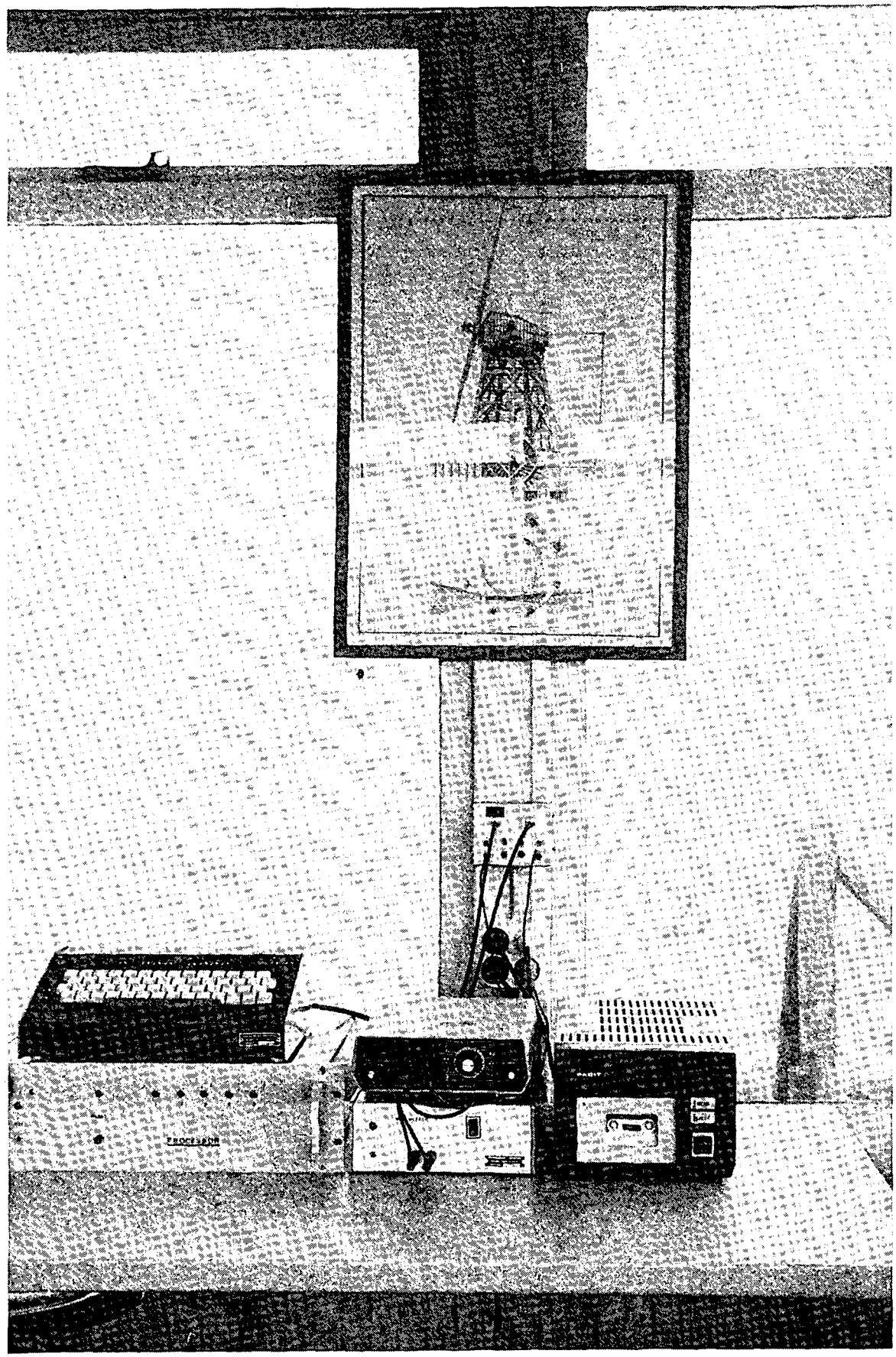

Fig. 36. The microprocessor system, under the eye of one of the windmill's ancestors. From left to right: the microprocessor with keyboard, the multiplexer with the digital voltmeter, and the cassette-recorder.

SWD PUBLICATIONS

Serial number		Price (incl. mail) US $	Dfl
SWD 76-1 (out of print)	Wind-energy utilization in Sri Lanka; potentialities and constraints. By A. Dennis Fernando and P.T. Smulders, 18 p., May 1976		
SWD 76-2	Literature survey; horizontal axis fast running wind-turbines for developing countries. By W.A.M. Jansen, 43 p., March 1976	3,–	6,–
SWD 76-3	Horizontal axis fast running wind-turbines for developing countries. By W.A.M. Jansen, 91 p., June 1976	7,–	14,–
SWD 76-4	L'énergie éolienne au Cabo Verde, une étude préparatoire des besoins et des possibilités de l'utilisation de l'énergie éolienne. Par J.C. van Doorn et L.M.M. Paulissen, 54 p., Août 1976	3,–	6,–
SWD 77-1	Rotor design for horizontal axis windmills. By W.A.M. Jansen and P.T. Smulders, 52 p., May 1977	4,–	8,–
SWD 77-2	Cost comparison of windmill and engine pumps. By L. Marchesini and S.F. Postma, 49 p., December 1978	4,–	8,–
SWD 77-3	Static and dynamic loadings on the tower of a windmill. By E.C. Klaver, 39 p., August 1977	4,–	8,–
SWD 77-4	Construction manual for a cretan windmill. By N. van de Ven, 59 p., October 1977	5,–	10,–
SWD 77-5	Performance characteristics of some sail- and steel-bladed windrotors. By Th. A.H. Dekker, 60 p., December 1977	5,–	10,–
SWD 78-1	Feasibility-study of windmills for Water Supply in Mara Region, Tanzania. By H.J.M. Beurskens, 89 p., March 1978	7,–	14,–
SWD 78-2	Savoniusrotors for waterpumping. By E.H. Lysen, H.G. Bos and E.H. Cordes, 42 p., June 1978	4,–	8,–
SWD 78-3	Matching of wind rotors to low power electrical generators. By H.J. Hengeveld, E.H. Lysen and L.M.M. Paulissen, 85 p., December 1978	7,–	14,–
SWD 79-1	Catalogue of windmachines By L.E.R. van der Stelt and R. Wanders, 41 p., September 1979	4,–	8,–

Research institutes in third world countries may ask for one copy free of charge max. 3 titles, writing directly to:

SWD,
c/o DHV Consulting Engineers,
P.O. Box 85,
3800 AB Amersfoort, The Netherlands

SWD publications can only be ordered by letter to SWD c/o DHV Consulting Engineers, P.O. Box 85, 3800 AB Amersfoort, The Netherlands
With a) your address in printing characters
b) requested titles

Payment: by cheque enclosed with your letter, or by remittance directly to DHV Consulting Engineers with Bank Mees en Hope, P.O. Box 293, Amsterdam, The Netherlands, acc. nr. 25.00.72.009 stating your name and address.